1-1-2012

The Effect of Relative Porosity on the Survivability of a Powder Metallurgy Part During Ejection

Daniel Ogbuigwe
Ryerson University

THE EFFECT OF RELATIVE POROSITY ON THE SURVIVABILITY OF A POWDER METALLURGY PART DURING EJECTION

by

Daniel Ogbuigwe

BASc Mechanical Engineering, Ryerson University, 2010

A Thesis presented to Ryerson University

in partial fulfillment of the requirements for the degree of

Master of Applied Science

in the Program of

Mechanical Engineering

Toronto, Ontario Canada, 2012

AUTHOR'S DECLARATION

I hereby declare that I am the sole author of this thesis. This is a true copy of the thesis, including any required final revisions, as accepted by my examiners

I authorize Ryerson University to lend this thesis to other institutions or individuals for the purpose of scholarly research

I further authorize Ryerson University to reproduce this thesis by photocopying or by other means, in total or in part, at the request of other institutions or individuals for the purpose of scholarly research.

I understand that my thesis may be made electronically available to the public.

THE EFFECT OF RELATIVE POROSITY ON THE SURVIVABILITY OF A POWDER METALLURGY PART DURING EJECTION

Master of Applied Science, 2012

Mechanical Engineering

Ryerson University

ABSTRACT

The desire to produce functional powder metallurgy (PM) components has resulted in higher compression forces during compaction. This in turn increases the ejection stresses and therefore the possibility of failure during ejection. This failure can be caused by sprig back during ejection due to frictional forces that are generated between the powder part and the die walls. In order to predict these factors a stress analysis of the powder part during ejection was done.

Due to complexity, finite element analysis was used to model the powder during compaction and ejection. Since the ejection stage is the most critical stage of the PM process, it is essential to understand the factors that determine the survivability of a part during this stage.

This work uses experimental data, finite element modeling and reliability analysis to determine the probability of failure of metallic powder components during the ejection phase. The results show that there is an increased possibility of failure during ejection as compaction pressure is increased. This information can be used by designers and process planners to determine the optimal process parameters that need to be adopted for optimal outcomes during powder metallurgy.

ACKNOWLEDGEMENT

I gratefully acknowledge the financial support from the department of Mechanical and Industrial Engineering at Ryerson University

I would like to thank my supervisor, Dr. Ahmad Ghasempoor, for his guidance and unfailing professional support from the beginning of my masters to the completion of this Thesis.

I appreciate the support from Dr. Hossein Kashanizadeh (Queens University) and PhD candidate Payman Ahi for engaging in discussions that related to my research and always being readily available for support and background information on relevant topics in powder metallurgy.

Finally, I am eternally grateful to my parents, siblings and most importantly God for providing me with both emotional and financial support throughout the duration of my graduate studies.

TABLE OF CONTENTS

List of Tables

List of Figures

Nomenclature

P/M	Powder Metallurgy
PDF	Probability Density Function
R	Cap Eccentricity
S_r	Survivability
d	Material Cohesion
p	Pressure
F	Applied Force (Load)
r	Random variable representing tensile failure stress
β	Angle of friction
σ	Tensile Failure Stress
v	Poisson's ratio
ρ	Correlation coefficient between variables p and v
σ_{pv}	Covariance between variables p and v
σ_p	Standard deviation of the variable p
σ_r	Standard deviation of the variable r for simulated 3 point bending
σ_v	Standard deviation of the variable v for Ejection Stress
μ_p	Mean value of the variable p
μ_r	Mean value of the variable r for simulated 3 point bending
μ_v	Mean value of the variable v for Ejection Stress

CHAPTER 1: INTRODUCTION

Powder metallurgy (PM) has become widely used and recognized as a robust process when producing high quality parts [1]. The process can be used for near net shape production of a wide variety of complex parts while providing energy savings, better material utilization and tailoring of properties.

Powder metallurgy involves two main stages, compaction and sintering. In the compaction stage, the powder is poured into a die that is of an approximate size and shape of the desired end product. The powder is then subjected to high pressures with punches to create the green compact where the particles bond together by mechanical interlocking and cold welding [2]. The green compact can be handled and machined, but the part is still weak. Sintering is when the green compact is heated to a temperature just below melting point causing the atoms in the powder to diffuse across boundaries of the powder particles which leads to the creation of a solid piece [2].

Before sintering occurs the part has to survive the ejection process before any manufacturing process can be performed on the part. The ejection is a critical stage in the production of a PM part. This is because the part has not yet been sintered making it weak and susceptible to fracture under loading caused by elastic recovery and the frictional forces between the die walls and the powder part [3]. Although stresses during ejection can be reduced using appropriate lubricants and mold design, the integrity of the green compact is still an issue. There are several areas of research dealing with the use of different compaction and ejection routes and various methods of compaction and unloading.

Since ejection is an important step in the manufacturing of powdered compacts, it is useful to explore the stress concentrations and reliability of the green compacts during ejection.

There have been many studies done on the analysis of compaction in powder metallurgy, but not on the ability of a part to survive the ejection process. In manufacturing and design today, reliability and quality assurance have become very important. Reliability analysis helps to determine the performance of a part and significantly affects the life cycle cost [4]. In complex systems, severe consequences can result from the failure of a single component, which is why it is vital to choose the best structural and mechanical characteristics in the design of a part. Therefore, it is important to know the failure behaviour and also the factors that cause these failures [5]. To achieve this in PM, finite element analysis in combination with experimental data helps to determine the stresses generated from the compaction to ejection step. The analysis of these stresses can be used to determine if a part would survive the ejection process. This work aims at predicting the survivability of parts based on their relative porosities and strengths during the ejection process. For this a simple test is proposed and the results of the test are used for calibrating a FE model. Principles of reliability analysis are then used for predicting the probability of failure during ejection from the die.

The thesis is organized as follows: Chapter 1 introduces powder metallurgy and how it relates to this thesis. Chapter 2 of this work will discuss the background of powder metallurgy and the existing work that has been done on powder compaction. Chapter 3 will provide the theory and methodology used to determine the survivability including the constitutive model used and the method for obtaining the necessary variables. Chapter 4 will show the finite element simulations of parts with different complexities and their stress distributions. Chapter 5 includes survivability computations and the case studies that show the survivability of different parts.

Chapter 6 will give the concluding remarks and give recommendations for future work.

CHAPTER 2: LITERATURE REVIEW

There have been several methods of pressing metallic powders into specific shapes. In prehistoric times, older civilizations used them for several applications including the iron pillar in Delhi, some Egyptian implements and articles of precious metals made by the Incas [6]. Industrial scale P/M started in the 1920s used for producing tungsten carbides inserts and the mass production of bronze bearings [6]. The use of powder metallurgy has continued to grow and develop into more efficient methods that improve the process. New types of powders with superior qualities have made it possible to produce larger and higher strength parts. Materials that used to be difficult to process like fully dense high performance alloys can now be produced with uniform micro structure [6].

Powder metallurgy is a sophisticated method that is used in manufacturing near net shaped components that can be used for various applications. P/M is done by blending elemental or pre-alloyed powders together, after which, this blend is compacted in a die followed by sintering of the pressed part in a controlled environment [2]. There are several advantages in using P/M. It can be used in the production of complex parts that require minimum secondary machining operations, the physical and mechanical properties can be tailored through a careful selection of starting materials and process parameters, and the properties can be improved through secondary processes like heat or cold treatments[3].

To improve the P/M method, further analysis into the stresses formed in the metallic powder particles need to be undertaken. There has been several research works that have used the combination of experimental data with complex mathematical computations to analyse the particle nature of powder [7]. Finite element analysis has been used to analyse powder as a continuous problem instead of a discrete problem. This has made the simulation of the powder metallurgy process possible.

2.1 Powder Metallurgy Process

In order to understand the PM process it is important to understand what happens to the powder particles during the compaction stage through to the ejection stage. There are several methods that have been used to analyse what happens to the powder. Some of these methods include the use of experiments to determine the material properties and their effect on the change from compaction to ejection with a combination of mathematical methods [7].

At the start of compaction, elastic deformation occurs at the point of contacts between punch and powder, and die walls and powder. As the pressure increases, the particles slide past each other and particle rearrangement occurs [8]. Plastic deformation also occurs and the flats on the surface of the particles increase in size. At higher pressures, rearrangement is no longer present, but plastic deformation continues and strain hardening is observed. At very high pressures, elastic deformation of the bulk material occurs, resulting in springback when the part is ejected from the die [8]. The forces generated within the compact due to springback can sometimes cause compact failure through cracking.

Some of the assumptions made when developing a model for powder compaction are:

(i) The homogeneity of the powder;

(ii) The size and shape of the particles, this depends on the type of technique used in making the powder which could include winning, deposition, atomization, fiber production and mechanical fiber production [3];

(iii) The temperature of the powder during compaction is usually assumed to be at room temperature and uniform.

The initial problem faced in analysing powder is the estimation of parameters that govern the progression of powder as it transforms into a solid part. In order to accomplish this, there has to be a combination of experimental data with mathematical modeling. Several procedures have been developed by researchers to take advantage of experimental data in determining parameters for constitutive models of powder compaction [9]. These methods are similar to those developed for soil testing.

There are four principal tests that can be used to develop a model these tests are: diametral compression test also known as Brazilian disc, uniaxial test, isostatic test and triaxial test [9]. After the material model is developed it becomes possible to simulate the process using finite element modeling. The most commonly used constitutive model is the Drucker Prager Cap Model which involves several parameters that can be used to analyse powder through simulations and material modelling.

Parameters that influence the survival of a part during ejection include friction between the part and the die [10], stresses in the part during ejection, complexity of the part, number of steps involved from compaction to ejection and the material properties.

To analyse the ejection stage there has to be an appropriate method that is capable of estimating the stresses involved during the process. There are two different approaches to the computational modeling of powder compaction and ejection: discrete and continuum modeling [7]. In the discrete method, each powder particle is treated individually by analyzing the surface interactions and deformations of each particle separately. While in the continuum method, the powder is treated as a continuous medium, which makes it more suitable for engineering applications [7]. The Drucker-Prager Cap model is a continuum model that enables powder compacts to be analyzed by finite element methods. Although the Drucker prager cap model is a suitable method for the analysis, the models have to be validated by comparing the porosity distribution and strength of the green compact with experimental results [11]. During compaction, the loose powder particles are transformed into a dense compacted state due to particle to particle bonds. There is also a weaker bond formed between the powder particles and walls of the die. During unloading and ejection of the part, the bond between the powder particles has to be greater than the bond between the powder and the walls of the die for a compact to be successfully ejected. These inter-particle bonds are dependent on the material type, temperature, method of compaction, and the relative porosity of the part. Relative porosity of P/M parts after compaction is also an important factor in the strength of the finished component. To achieve the appropriate relative porosity, the kinematics of punches and applied forces play a vital role. These compaction forces and relative porosity together with part geometry in turn determine the stresses developed during ejection step.

2.2 Modeling of Powder Metallurgy Process

Bejarano [12] used Abaqus finite element software to simulate cold compaction of a two-level powder metallurgical part. To model the plastic behavior of these metallic powders, the Drucker-Prager Cap model was used. A pseudo-linear model of elasticity was applied to simulate the ejection process[12].

Although Drucker-Prager Cap model seems to be the most appropriate method for representing the behavior of materials in powder compaction, most of the materials being studied show plastic strain in the first stages of the loading surface which is contrary to the straight line section of the Drucker-Prager Cap [8]. The illustration in Figure 1 shows that plasticity begins much earlier than anticipated. But this was only within a small section towards the end of the Drucker-Prager Cap model, and was considered an acceptable approximate.

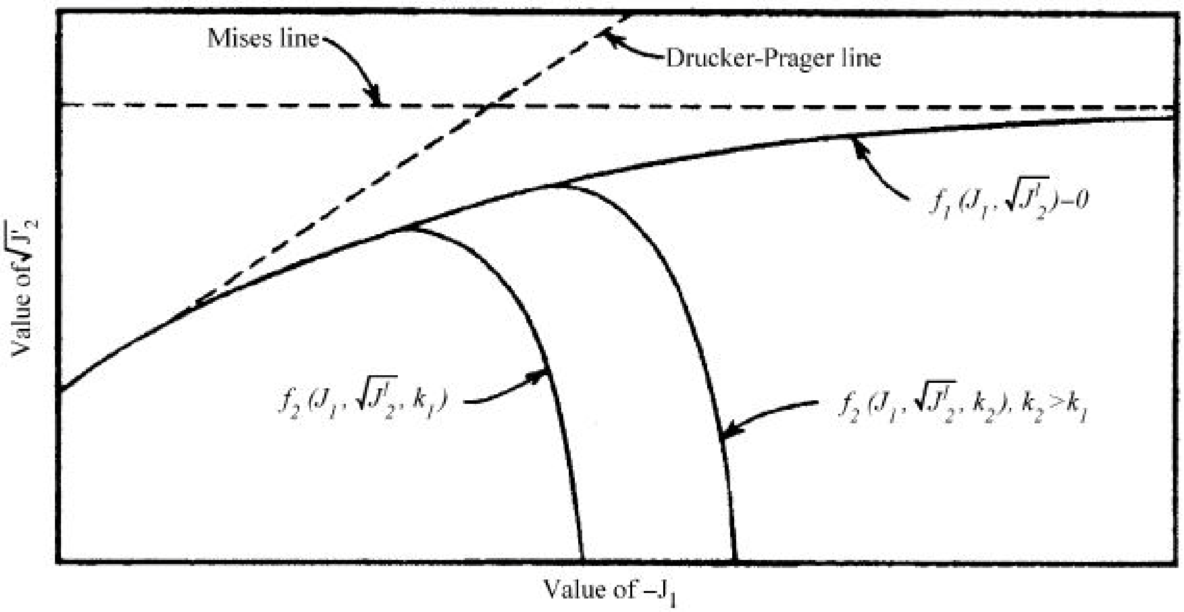

Figure 1: Caps and failure surface in the CAP plasticity model [8]

To simulate the creation of a part through powder metallurgy [8], two steps were used, the compaction step and ejection step. The diagram in Figure 2 shows how the steps were implemented with a series of punches:

1. Compaction: a symmetric part was compressed with individual punches as shown in Figure 2.

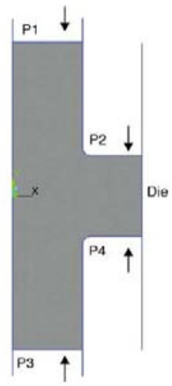

Figure 2: Powder and compaction tools [8]

2. Ejection: during this phase each punch is removed progressively with exemption of the punch 3 which is at the bottom of the part as shown in Figure 3

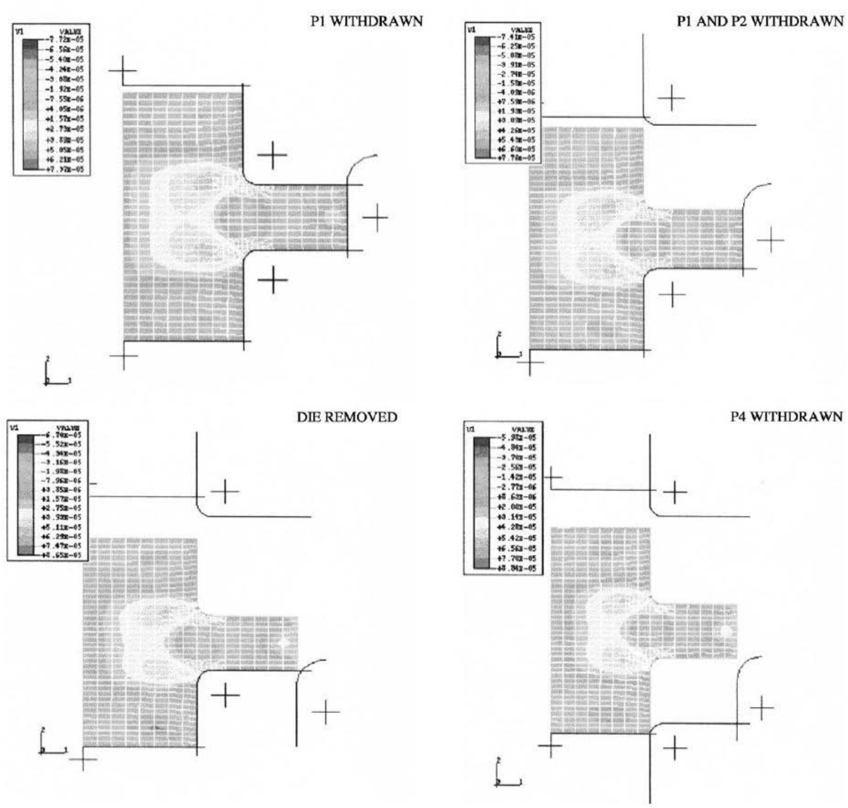

Figure 3: Progressive spring-back during the ejection stage [8]

During the simulation and fabrication of this tool, the main problem encountered in the simulations was representing the gradients of density during the filling stage; this issue was ignored in the simulation by assuming a homogeneous initial distribution of density. In the ejection phase of the simulation, spring back was noticed which can cause fractures in the compact. The 4 punches used in this simulation were chosen and were removed simultaneously to minimize stress within the compact.

Drucker-Prager was found to be suitable in representing the expected responses during the compaction and ejection of a metallic powdered part, providing much more information than in the experimental data [8].

It was proposed that different compaction and ejection routes would result in different stress distributions within the part [11]. The focus was also on cold die compaction where plastic deformation of the powder particles was the major deformation process. This research was to analyze how fragile the component might be after ejection from the die. In the beginning of the compaction process after the particles had deformed, porosity existed in form of isolated voids. Further study showed that porosity depends not only on inter-particle cohesive strength but also on applied loads resulting from the punches and the die. The effects of these loads also depend on parameters such as matrix material behavior, friction between die and powder material, and other compaction parameters [11]. The maximum principal stress during compaction and ejection was determined to give insight into the risk of fracture during the process by simulating different compaction and ejection routs and also varying the speed ration of the punches. The ejection in the model was simulated by removing one of the punches and then using the opposite end to eject the part from the die. The distribution of residual stresses was determined as a function of cohesion in order to determine whether the difference of residual stresses during compaction also exists after ejection from the die [11].

It was found that ejecting the specimen from one side or the other affects the residual stress distribution [11]. However, the residual stress was mainly due to the externally applied axial pressure from the inner punch, during ejection. A simple boundary unloading method provided a useful guide in predicting the residual stress distribution but it did not capture the evolution of the maximum principal stress during ejection which may have exceeded the final value in the specimen when completely ejected from the tool.

Other researchers have explored various factors that affect the compaction and ejection of powder. One of which was the effects of friction on powder compaction. Many of the final properties of the manufactured P/M components have shown to be strongly dependent on the wall friction between the die and the powder component [10]. The quantification of the wall friction evolution over the whole density range of the powder is complicated and closely connected to the material behavior. Measuring local contact stresses is difficult because stresses at the contact zone are usually not directly accessible from the measurements. The frictional shear stress at the contact interface was computed according to Coulombs friction law, depending on density or velocity of the powder [10]. To determine the effects of friction between the walls and the powder, strain gauges were positioned on the outer container surface. The friction values that were estimated, depended on the surface finish and the lubricant with the friction coefficient kept between μ=0.05 and 0.25 [13].

Another factor that has been studied is the green density. The green density is a function of the applied pressure and the instantaneous axial compression strain. This strain can be estimated from the incompressibility condition, where the mass of the powder is constant at all times [13]. The green density is equal to the tap density plus the increase in densification due to compaction. The influence of the powder/wall friction on the axial density distribution was obtained from a plot of density at different height locations [13]. These effects can be seen in Figure 4.

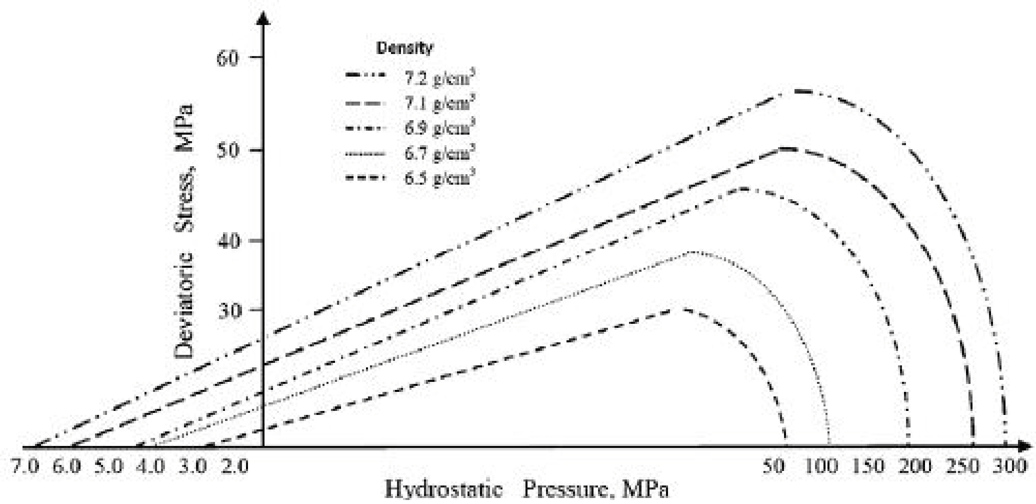

Figure 4: DPC model yield surface and the effects of density [10]

It can be noticed from the previous work on powder metallurgy that the most prominent constitutive material model for simulating powder compaction and ejection is the Drucker-Prager Cap model (DP). Most of the Drucker-Prager parameters are obtained from experimental data. To completely utilize the DP model, it is assumed to be isotropic and has three yield surfaces which include a shear failure surface (F_s); a cap plasticity surface, (F_c); and a transition surface, (F_t). These three surfaces make it possible to simulate the densification and hardening of powder. In some cases, triaxial equipments have been used to calibrate the Drucker-Prager cap model [14]. The triaxial equipments are complex and difficult to use in practical engineering applications, which is why calibration methods based on experiments from compaction simulations are used [7].

During the unloading phase, since the passion's ratio and Young's modulus are assumed to be constant, Drucker-Prager model is not suitable for simulation and analysis of the nonlinear unloading behavior of powder. This results in approximate modeling of the elastic recovery during the unloading and ejection steps. Due to these factors, the creation of cracks during the elastic recovery after unloading cannot be properly simulated using the Drucker-Prager cap model [7]. Due to these shortcomings, the addition of certain other characteristics like elasticity, density, and some other material properties that aid in the analysis of the full compaction cycle (compaction-Unloading-ejection) is necessary.

An important aspect of Drucker-Prager Cap Model is the yield surface. The yield surface provides a boundary at which the yield point is reached [15]. Usually, the yield surface is expressed in terms of a three dimensional principal stresses (σ_1, σ_2, and σ_3) and a two or three dimensional space spanned by stress invariants (I_1, J_2, and J_3). Therefore, the yielding surface can be written as: $f(\sigma_1, \sigma_2, \sigma_3) = 0$, $f(I_1, J_2, J_3) = 0$ With I_1 as the first principal invariant of Cauchy stress and J_2, *and* J_3 as the second and third principal invariants of the deviatoric part of the stress tensor.

The Drucker-Prager yield criterion can then be written as [15]:

$$F(\sigma) = \alpha I_1 + \sqrt{J_2} \qquad (1)$$

Here, α is a material constant that can be related to the friction angle, φ, and cohesion, c.

The Drucker-Prager failure surface is described by:

$$F_s = t - p\tan\beta - d = 0 \qquad (2)$$

The parameters for equation (2) are:

β = the angle of friction

d = the material cohesion sometimes denoted as c; and

p = the equivalent pressure stress related to the stress tensor

The cap region has an elliptical shape describing the cap yield surface as [16]:

$$F_c = \sqrt{[p - p_a]^2 + [\frac{R_t}{1 + \propto - \propto / cos\beta}]^2} - R(d + p_a tan\beta) = 0 \qquad (3)$$

Where, *R* is the ratio of the length to the height of the elliptical cap when ignoring the transition region; it controls the eccentricity of the cap; p_a is the hardening function driven by volumetric inelastic-strain. Figure 5 shows a graphical representation of the Drucker-Prager cap model

The Drucker prager model of plasticity is a good representation of the compaction of metallic powders, but there has been a shortage in experimental data, especially with regards to failure [8]. Most of the previous research showed that the ejection of the compact was a critical stage. The materials used in cold powder compaction are porous and therefore are not able to carry large tensile stresses due to the weak bonds between powder particles [11]. This results in failure when the porous aggregate is subject to tensile stresses that exceed a certain limit. This failure is usually a brittle fracture depending on the maximum principle stresses. During the ejection process, maximum principle stresses occur that are higher than the final maximum stresses of the unloaded part [11]. Figure 6 shows that during most of the compaction and ejection, the parts of the compact that are susceptible to maximum principle stresses are located at the corners or rounded edges.

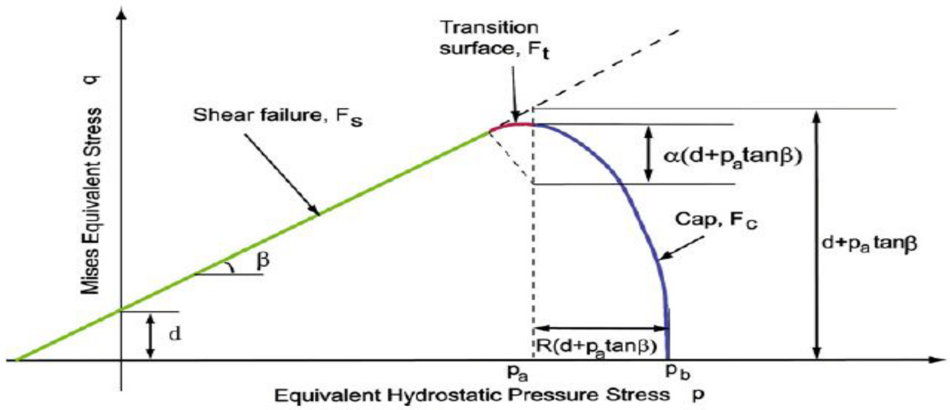

Figure 5: Drucker-prager Cap Model: yield surface in the p-q plane [7]

In some cases the highest stress concentration occurs at the outer sides of the powder part that make the last contact with the die walls as the compact is ejected [11].

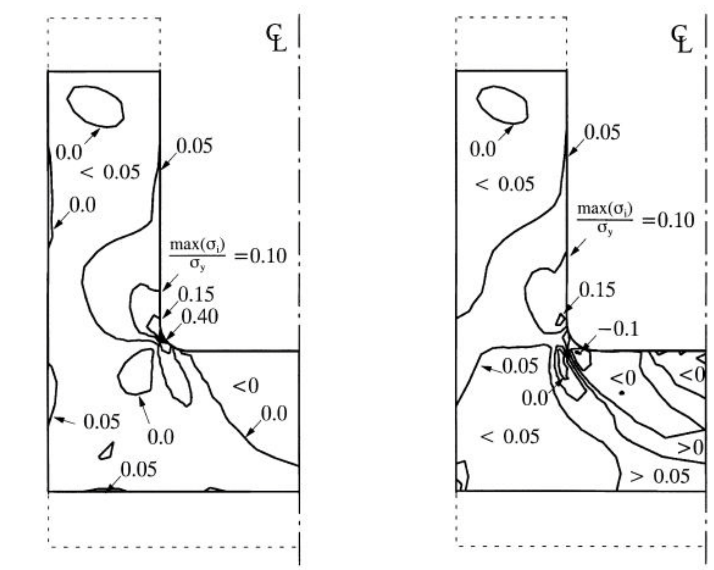

Figure 6: Curves of constant maximum principal stress [11]

There are many factors that can cause failure of a part during ejection, which is why it is important to consider the reliability of components/parts made by powder technology. The brittle fracture that occurs in PM can be described by a probabilistic model with the assumption of weakest link hypothesis [17]. The hypothesis states that the failure of a structure occurs when one element fails, but this hypothesis was improved to include physical data such as the distribution of defects to describe what happens at the failure point when there is a re-distribution of stresses [18]. This lead to estimating the probability of failure based on a given deterministic loading history, with the material creep life and fatigue life as random variables[19]. This approach was extended by including the number of creep and loading cycles and was used to provide probability density function curves of creep and fatigue life that corresponded to different stress/strain levels at different temperatures [20]. The graphs in Figure 7 show the fatigue life probability density function (PDF) curves and the fitted stress-creep life curves.

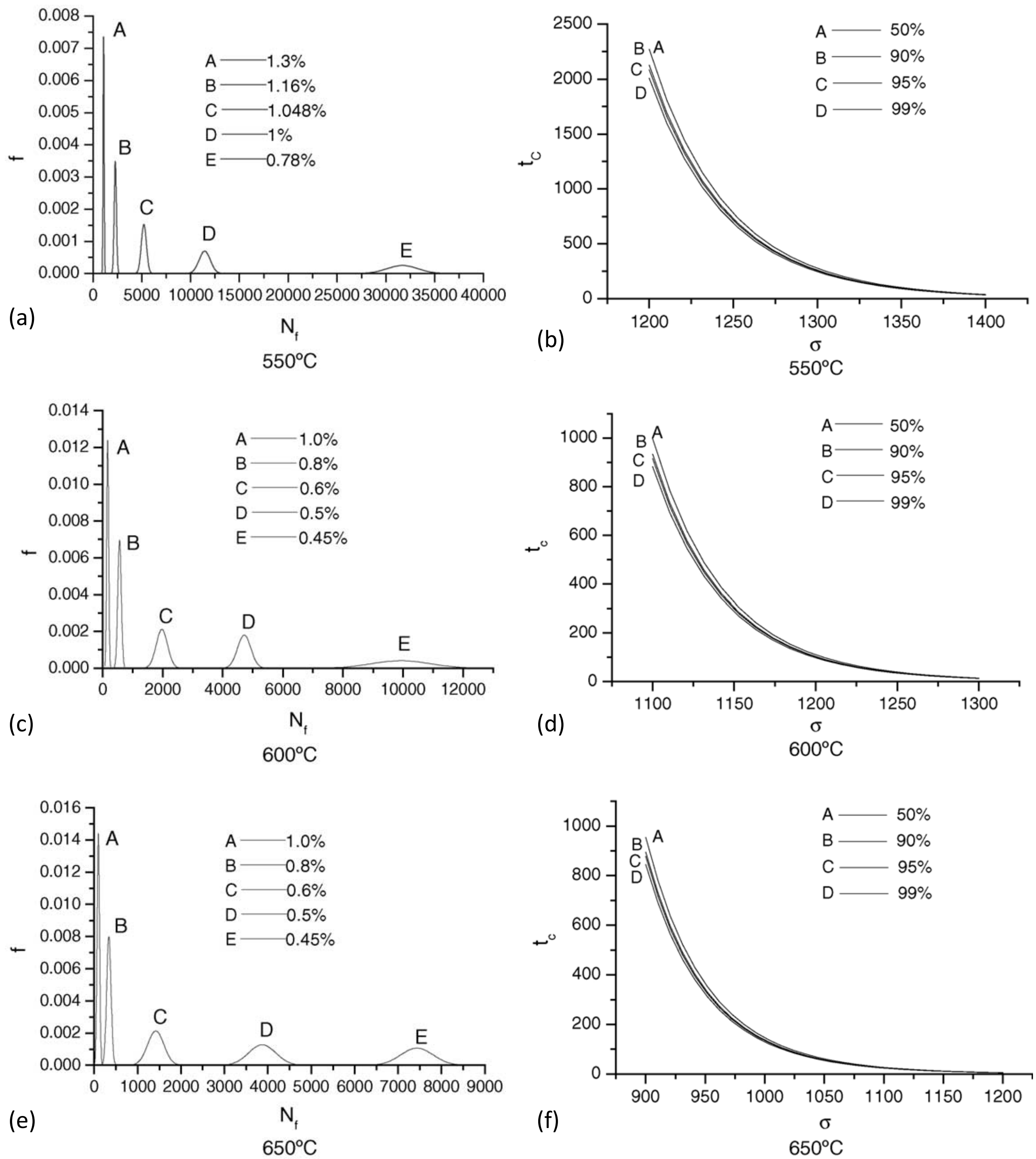

Figure 7: The fatigue life PDF curves at different strain ranges (graphs a, c, and e) and the fitted stress-creep life curves at different confidences (graphs b, c, and f) [20]

Fatigue and creep have been the most concentrated subject areas that have been researched for reliability and lifetime predictions of components made by PM technology. But most of these reliability studies have been on the sintered component and not on the reliability of the green compact. The review of the literature showed that there is very little material on the analysis of the ability of a part to survive the ejection process. Although some of the research shows the stresses in the ejected part, they don’t show much detail on the effects of relative porosity on the survivability of the ejected part. To further understand what happens after ejection it is important to predict the survivability of a part during the ejection process, which would help in fully understanding the P/M process. But before this analysis can be done the finite element model used has to be fully explored to be able to correctly simulate the P/M process. The finite element method used in this research makes use of the Drucker Prager Cap model.

CHAPTER 3: METHODOLOGY

In this chapter finite element modeling is combined with the reliability approach to determine the probability of a cold compact surviving the ejection stresses.

3.1 Survivability

Since parts that are made with powder metallurgy process are usually weakest during the ejection phase, it is useful to determine the survivability of a part during ejection, especially when high compaction pressures are used to increase density. Using a mathematical survivability model helps to carry out this reliability analysis by considering the important factors involved in the compaction and ejection of powder parts.

Using the Probability Density Function (PDF) to represent the strength of the part and the ejection stresses, it is possible to create a joint PDF to use as an indicator of survivability.

The PDF for the strength of the part can be determined by using the maximum tensile stress before failure (tensile strength) and can be defined as:

$$F(v) = \int_0^{\hat{v}} f(v) d_v \qquad (4)$$

Similarly, the PDF for the maximum ejection stress, which can be extracted directly from the FE model during the ejection simulation, can be defined as:

$$F(r) = \int_0^{\hat{r}} f(r) d_r \qquad (5)$$

Therefore, the joint PDF constructed from Equations 4 and 5 forms the survivability equation which is:

$$S = \int_{\hat{v}}^{0} f(v) \left[\int_{0}^{r} f(r) d_r\right] d_v \qquad (6)$$

In this work all the parameters in the proposed survivability model *(v and r)* are assumed to be normally distributed. Therefore *f(v) and f(r)* are defined as follows:

$$f(v) = \frac{1}{\sigma_v \sqrt{2\pi}} e^{-\frac{(v-\mu_v)^2}{2\sigma_v^2}} \qquad (7)$$

where,

$$\sigma_v = \frac{1}{n-1} \sum_{i=1}^{n} (v_i - \mu_v) \qquad (8)$$

Similarly,

$$f(r) = \frac{1}{\sigma_r \sqrt{2\pi}} e^{-\frac{(r-\mu_r)^2}{2\sigma_r^2}} \qquad (9)$$

where,

$$\sigma_r = \frac{1}{n-1} \sum_{i=1}^{n} (r_i - \mu_r) \qquad (10)$$

Substituting Equations 7-10 in Eq. 6 yields:

$$S = \int_{\hat{v}}^{0} \frac{1}{\sigma_v \sqrt{2\pi}} e^{-\frac{(v-\mu_v)^2}{2\sigma_v^2}} \left[\int_{0}^{\hat{r}} \frac{1}{\sigma_r \sqrt{2\pi}} e^{-\frac{(r-\mu_r)^2}{2\sigma_r^2}} d_r\right] d_v \qquad (11)$$

Equation 11 is used for computing the survivability. It can be seen that the survivability model depends mainly on two variables, *v* and *r*. To analyze the survivability of a part during ejection, there are two important properties that will be used as these two variables, they include:

- The maximum stresses in the part during the ejection process,
- And the tensile strength of the ejected part

These two properties would make it possible to establish the survivability of the ejected part (green compact) by comparing the relationship between the ejection stress and the strength of the ejected part. This would help determine if a part would survive the ejection process. For a part to survive, the ejection stresses would have to be less than the tensile strength of the part. This is what would be used to determine the survivability of a part.

Although parts with higher densities have better mechanical properties, they have a higher risk of having high ejection stresses [21], which could lead to failure during ejection. Since determining the stresses developed during ejection experimentally are not feasible, finite element modeling will be used to determine the stress distribution in the green compact during ejection.

Three point bend tests are commonly used to determine the strength of a green compact [22] although there are a variety of other tests that can be used in determining strength, it was chosen for its direct and straight forward implementation in the prismatic part used during this thesis. In this work, the results of three point bend tests are also used to calibrate the FE model. Prismatic specimens made with various compaction pressures and different relative porosities were prepared and the three point bend test was carried out on the green compact right after ejection.

The experiments were also simulated as shown in Figure 8. The steps in simulation were; the compaction step, were the two punches were used to compress the part simultaneously; the unloading and ejection stage, were the punch 1 was removed and punch 2 was used to eject the part; and the 3 point bend test which was done on the ejected part until failure occurred.

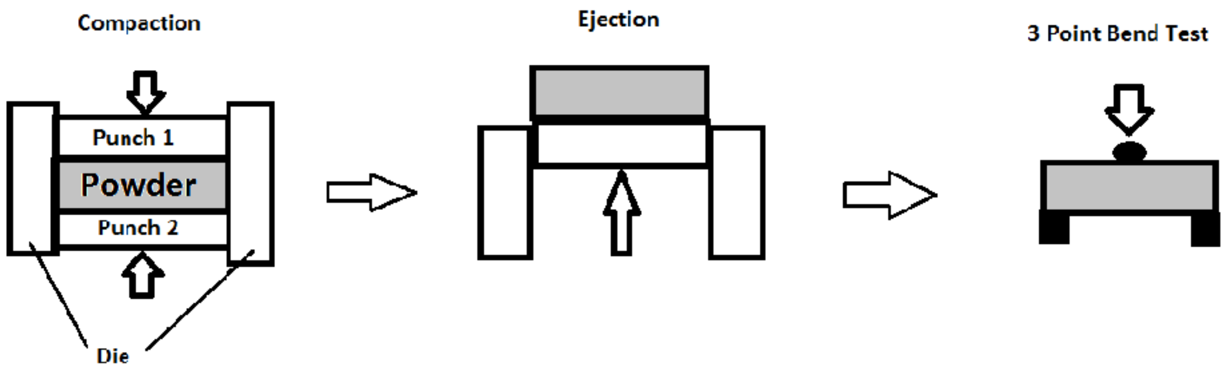

Figure 8: Steps involved in determining the strength of green compact

The part dimensions are shown in Figure 9

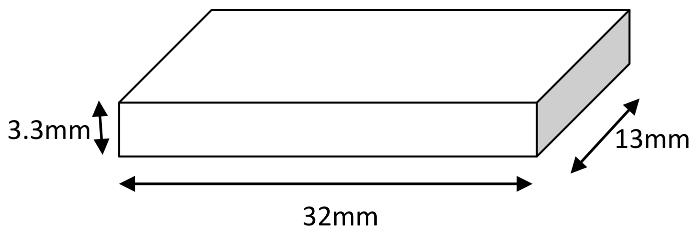

Figure 9: Prismatic Specimen for 3-Point Bending Test

The values for the maximum tensile stress was obtained by performing a three point bend test on the ejected part which was done right after ejection of the part. This was repeated for 25 parts with different relative porosities. Before the 25 parts were simulated, the parameters had to be determined. And since only the material was known, the other parameters needed in the Drucker Prager cap model had to be determined by a different approach.

3.2 Determining Parameters for Finite Element Model (Calibration)

In order to use FE modeling of compaction and ejection it was important to determine the proper parameters to be used for the Drucker Prager cap model. The Drucker-Prager material model has linear and non-linear parts. Therefore it has to be computed by integrative numerical schemes.

The linear section of the Drucker-Prager material model is defined by [7]:

$$F_s = q - p\ tan\beta - d = 0 \qquad (12)$$

For a uniaxial die compaction test, the hydrostatic and the Von Mises equivalent stress are expressed as [23]:

$$p = -\frac{1}{3}(\sigma_z + 2\sigma_r) \qquad (13)$$

$$q = |\sigma_z - \sigma_r| \qquad (14)$$

As mentioned earlier, the cap yield surface is written as [7]:

$$F_c = \sqrt{[p - p_a]^2 + [\frac{R_t}{1 + \alpha - \alpha/cos\beta}]^2} - R(d + p_a tan\beta) = 0 \qquad (15)$$

$$p_a = \frac{p_b - Rd}{(1 + Rtan\beta)} \qquad (16)$$

$$p_b = f(\varepsilon_v^p) \qquad (17)$$

$$\varepsilon_v^p = \ln\left(\frac{\rho}{\rho_0}\right) \qquad (18)$$

The transition surface from the linear section to the elliptical section is defined by [7]:

$$F_t = \sqrt{[(p - p_a)]^2 + [q - (1 - \frac{\alpha}{cos\beta})(d + p_a tan\beta]^2} - \alpha(d + p_a tan\beta) = 0 \qquad (19)$$

The plastic flow rule can be determined by a potential function for both the cap region Gc and the transition region Gs [23].

$$G_c = \sqrt{(p-p_a)^2 + \left[\frac{Rq}{1+\alpha-\alpha/cos\beta}\right]^2} \qquad (20)$$

$$G_s = \sqrt{[(p-p_a)tan\beta]^2 + \left[\frac{q}{1+\alpha-\alpha/cos\beta}\right]^2} \qquad (21)$$

G_c and G_s are the two elliptical portions that form a continuous and smooth potential surface.

The inelastic strain rate in the cap region can be written as [7]:

$$\dot{\varepsilon}_{ij}^{p} = \dot{\lambda}\frac{\partial G_c}{\partial \sigma_{ij}} = \dot{\lambda}\frac{\partial F_c}{\partial \sigma_{ij}} \qquad (22)$$

$\dot{\lambda}$ is a positive scalar that represents the magnitude of the plastic deformation and $\frac{\partial G_c}{\partial \sigma_{ij}}$ represents the direction of plastic flow.

Parameters needed to define each yield surface are:

1. For shear failure:
   - The friction angle β
   - Cohesion *d*
2. Cap Surface:
   - Cap eccentricity parameter, *R* is between 0.0001 and 1000.0 but most materials have it less than 1.
   - Evolution (pressure) p_a represents the volumetric plastic strain hardening/softening
3. Cap hardening:
   - p_b which is a function of volumetric plastic strain is the hydrostatic compression yield stress

4. Transition Surface requires α (typically between 0.01-0.05)

The elastic parameters for the Drucker-Prager cap model require the use of the Young's modulus, *E*, and the Poisson's ratio, *v*, which are related to the Bulk modulus, *K*, and the shear modulus, *G*, by the equations below:

$$G = \frac{E}{2(1+v)} \qquad (23)$$

$$K = \frac{E}{3(1-2v)} \qquad (24)$$

Using the stress tensor σ_{ij} which can be expressed in terms of two other stress tensors::

$$\sigma_{ij} = s_{ij} + p\delta_{ij} \qquad (25)$$

Here *p* is given by [24]:

$$p = \frac{\sigma_{kk}}{3} = \frac{\sigma_{11}+\sigma_{22}+\sigma_{33}}{3} = \frac{1}{3}I_1 \qquad (26)$$

The deviatoric stress tensor s_{ij}, can be obtained by solving the matrix [24]:

$$\begin{bmatrix} s_{11} & s_{12} & s_{13} \\ s_{21} & s_{22} & s_{23} \\ s_{31} & s_{32} & s_{33} \end{bmatrix} = \begin{bmatrix} \sigma_{11} & \sigma_{12} & \sigma_{13} \\ \sigma_{21} & \sigma_{22} & \sigma_{23} \\ \sigma_{31} & \sigma_{32} & \sigma_{33} \end{bmatrix} - \begin{bmatrix} p & 0 & 0 \\ 0 & p & 0 \\ 0 & 0 & p \end{bmatrix} \qquad (27)$$

$$\begin{bmatrix} s_{11} & s_{12} & s_{13} \\ s_{21} & s_{22} & s_{23} \\ s_{31} & s_{32} & s_{33} \end{bmatrix} = \begin{bmatrix} \sigma_{11} - p & \sigma_{12} & \sigma_{13} \\ \sigma_{21} & \sigma_{22} - p & \sigma_{23} \\ \sigma_{31} & \sigma_{32} & \sigma_{33} - p \end{bmatrix} \qquad (28)$$

Using the incremental hooks law we can compute the elastic strain increments by [23]:

$$d\varepsilon_{ij}^{e} = \frac{dI_1}{9K}\delta_{ij} + \frac{ds_{ij}}{2G} \qquad (29)$$

Where $I = 3p$ from equation (26) which is the first stress invariant, $\sqrt{J_2} = q/\sqrt{3}$ which is the second stress invariant. For axial strain loading, equation (29) becomes:

$$d\varepsilon_z = \frac{d\sigma_z + 2d\sigma_r}{3K} = \frac{dp}{3}\frac{1}{K} \qquad (30)$$

$$d\varepsilon_z = \frac{d\sigma_z + d\sigma_r}{2G} = \frac{dq}{2G} \qquad (31)$$

At the loading point, which is when F_c = 0, the radial plastic strain rate from equations (22) becomes:

$$\dot{\varepsilon}_{ij}^{p} = \dot{\lambda}\frac{\partial G_c}{\partial \sigma_{ij}}|_{(p,q)} = 0 \qquad (32)$$

And since $\dot{\lambda}$ is a positive quantity, we can isolate the partial derivative:

$$\frac{\partial G_c}{\partial \sigma_{ij}}|_{(p,q)} = 0 \qquad (33)$$

And equation (20) at this point becomes:

$$2(p - p_a)\frac{\partial p}{\partial \sigma_r} + 2\frac{R^2 q}{(1+\alpha-\frac{\alpha}{\cos\beta})^2}\frac{\partial q}{\partial \sigma_r} = 0 \qquad (34)$$

Since $p = 1/3(\sigma_z+\sigma_r)$ and $q = |\sigma_z-\sigma_r|$, and if at $F_c=0$, $p=p_A$ and $q=q_A$, equation (34) becomes:

$$\frac{2}{3}(p_A - p_a)\frac{\partial p}{\partial \sigma_r} + 2\frac{R^2 q_A}{(1+\alpha-\frac{\alpha}{\cos\beta})^2}\frac{\partial q}{\partial \sigma_r} = 0 \qquad (35)$$

This makes the cap parameter R to be:

$$R = \sqrt{\frac{2\left(1+\alpha-\frac{\alpha}{\cos\beta}\right)^2}{3q_A}(p_A - p_a)} \qquad (36)$$

Equations 12 to 36 form the foundation for analyzing the processes involved in powder metallurgy and is used in the finite element computations that govern the simulation of the compaction and ejection of a powder compact. There are several parameters for the three regions. The main parameters for the shear failure region are the friction angle (β) and the cohesion (*d*); the main parameters for the cap surface are the cap eccentricity parameter (*R*) which is less than 1 for most materials, and the evolution (pressure p_a) which represents the volumetric plastic strain hardening/softening; the main parameter for the cap hardening region is the hydrostatic compression yield stress (p_b) which is a function of volumetric plastic strain.

Most of the Drucker-Prager parameters are obtained from experimental data. To completely utilize this model up to the ejection phase, the model is assumed to be isotropic. Ideally, triaxial equipment should be used to calibrate the Drucker-Prager cap model. However, the triaxial equipment is complex and difficult to use. In this study three point bending experiments were used for the calibration of the FE model.

Five iron powder compacted samples with dimensions shown in Figure 9 were made. These were produced with different relative porosities ranging from 44.05% to 9.47%. The samples were put through three point bending tests to determine the maximum tensile strength. The procedure to calibrate the FE model consisted of finding the combination of Drucker Prager model parameters that will result in FE model matching the experimental values for strength. A designed experiment approach with analysis of means was used.

Each parameter was studied at three levels within a feasible range for that parameter (Table 2). The combinations of these levels were determined by a Taguchi orthogonal array L-$_9(3)^4$ (9 runs, 4 variables, 3 levels) as shown in Table 1 [25].

Table 1: Experimental design for $L_9(3)^4$ orthogonal array

Experiment	Variable 1	Variable 2	Variable 3	Variable 4
1	A1	B1	C1	D1
2	A1	B2	C2	D2
3	A1	B3	C3	D3
4	A2	B1	C2	D3
5	A2	B2	C3	D1
6	A2	B3	C1	D2
7	A3	B1	C3	D2
8	A3	B2	C1	D3
9	A3	B3	C2	D1

Table 2: Material property values

Level	Density	Cap eccentricity	Angle of friction	Material cohesion
1	3.15	0.3	35	0.3
2	4.72	0.6	60	0.6
3	1.57	0.8	75	0.7

This combination was repeated for each of the 5 relative porosities. The FE model was run by using each combination of the Drucker Prager parameters. The maximum tensile strength for each combination was recorded and compared with the tensile failure stress obtained from the experimental results (Table 5 Appendix A). The combination results are shown in Table 6 of Appendix A. The error was defined as the squared difference between the simulated results and experimental values.

The analysis of mean was used to find the best combination for the material properties shown in Table 3 by selecting the values that resulted in the minimum squared difference. These material properties were used in all the following finite element simulations. The values obtained from the analysis of means were close enough to the expected values, the relationship is shown in Figure 11. The strength of the 25 parts was determined by the three point bend test shown in Figure 10. Each of these parts had different relative porosities. The results from the simulation were plotted with the results from the experimental data. Figure 11 shows the relationship between simulated and the experimental results.

Table 3: Table showing the selected material properties combination in bold.

Trial	Density	Cap eccentricity	Angle of friction	Material cohesion
1	**3.15**	**0.3**	35	0.3
2	4.72	0.6	60	0.6
3	1.57	0.8	**75**	**0.7**

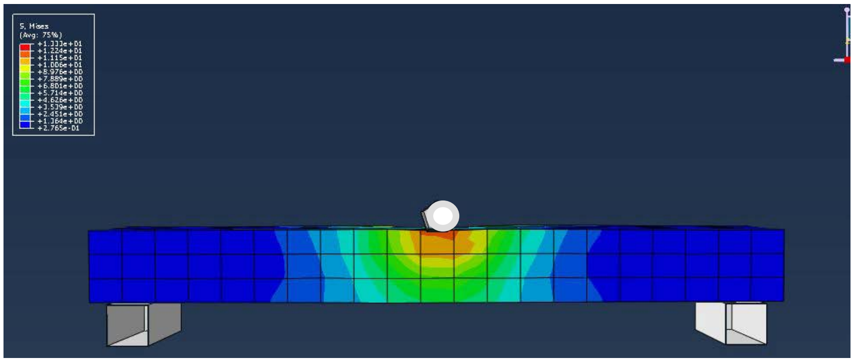

Figure 10: 3 Point Bend showing maximum stress distribution

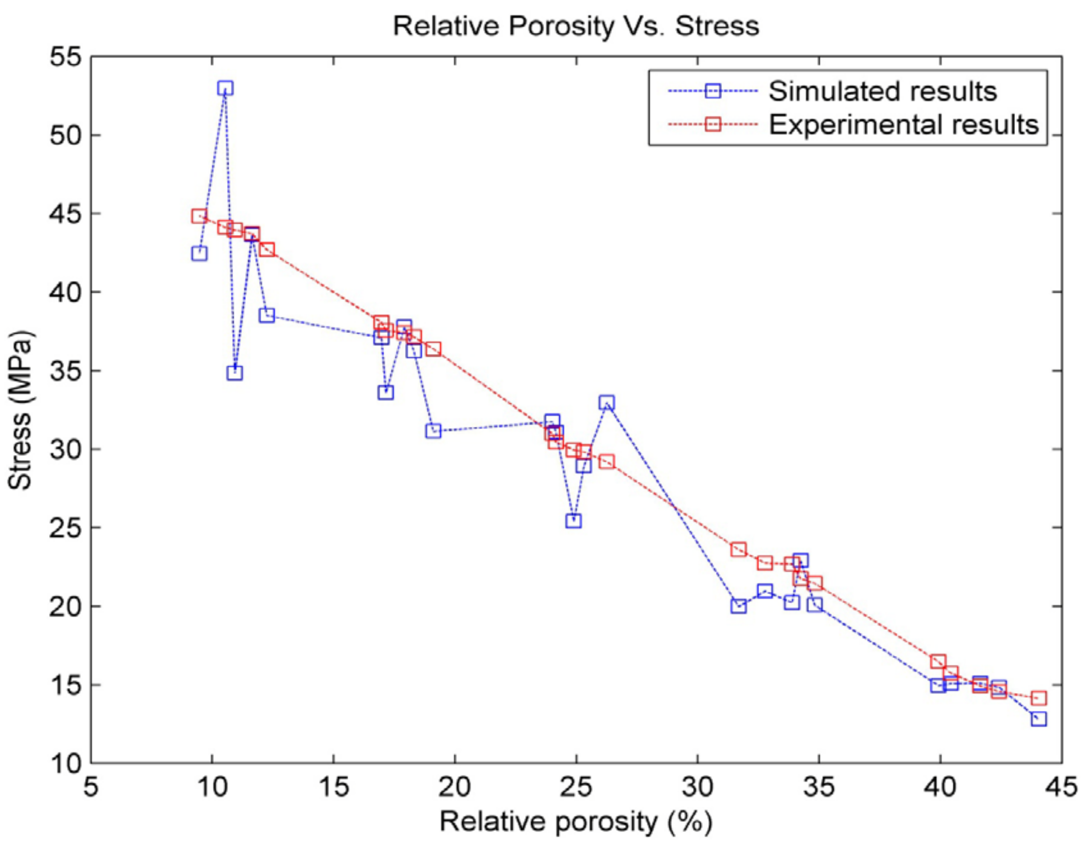

Figure 11: Graph showing relationship between the experimental results and simulated results of the maximum tensile stresses of prismatic part.

The simulated results show a good estimate of what the maximum stresses would be. The values were simulated in groups of five, so although some of the values may seem a little irregular, the relationship between the average simulated values and the average experimental values shown in Figure 12 show that the simulated results are very close to the experimental values and therefore and acceptable way to estimate the stresses induced in the PM part.

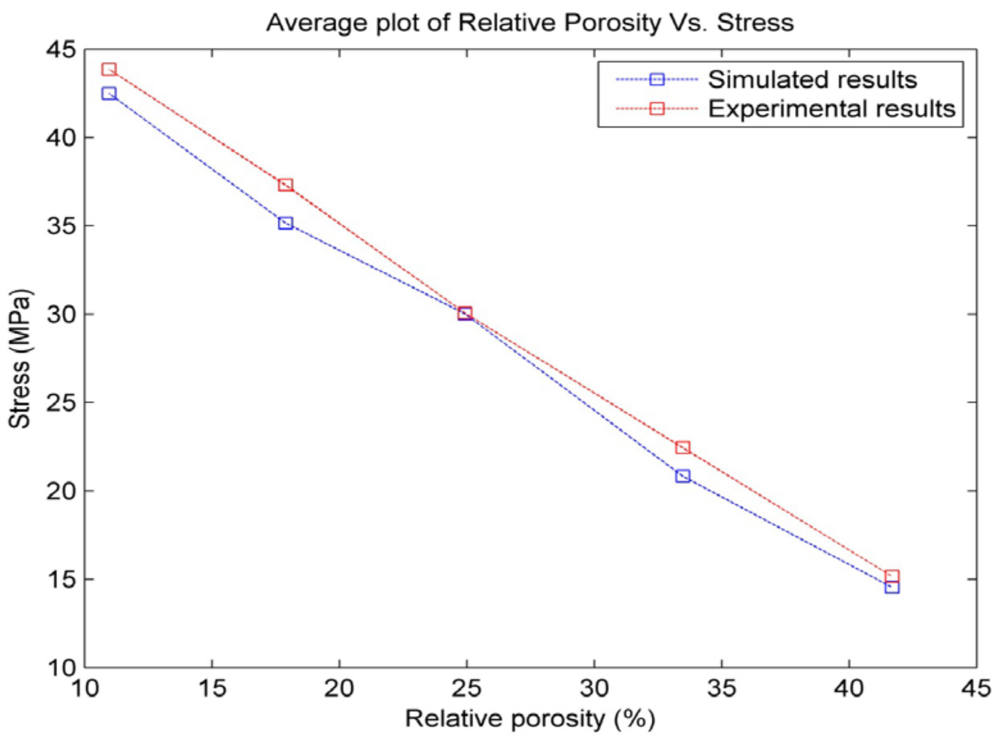

Figure 12: Graph showing average maximum stress values of the maximum tensile stresses of prismatic part

Another parameter that had to be determined was the initial height. To obtain the required initial height, the relative porosity, density and the final height were used since they were already known. The initial height of the rectangular specimen was calculated as follows:

$$initial\ hight = \frac{final\ hight \times (100 - relative\ porosity) \times density\ of\ iron}{initial\ density}$$

The only variable in the above equation was the relative porosity which was selected to be similar to that of the experimental data.

After the calibration of the finite element model parameters was done, the values obtained were used for all following simulations.

CHAPTER 4: FINITE ELEMENT SIMULATIONS

Finite element modeling was used to simulate the different steps involved in the making of a PM part. Several types of parts were modelled, ranging from cylindrical parts to gears, in order to explore the stresses involved in ejection of components of different complexities.

4.1 Cup Model

The first part that was modeled was a cylindrical cup. Figure 13 shows the schematic representation of the arrangement of the punches and the die with respect to the powder. The modelling was done using two different approaches: two-dimensional (Axisymmetric) approach and three-dimensional approach.

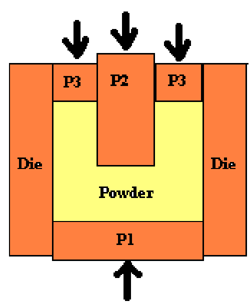

Figure 13: Schematic of Compaction Sequence

4.1.1 Axisymmetric Model

The diagrams in Figure 14 and Figure 15 show the axisymmetric simulations of a cup model. This was simulated using the triangular elements.

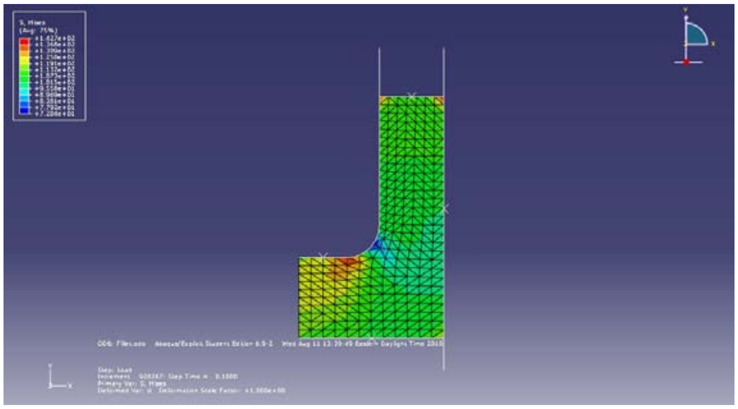

Figure 14: compaction for the Axisymmetric model

Figure 15 shows the axisymmetric model which involved the removal of the top punch and the center punch.

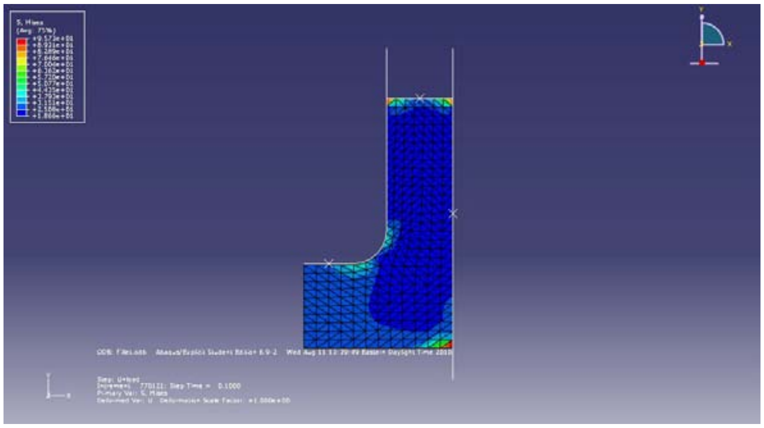

Figure 15: unloading for Axisymmetric model

Figure 14 and Figure 15 shows that the areas with the maximum stress concentration are in the corners which are as expected. The simulation was done with triangular elements which are the most appropriate element type for this particular model and part shape, triangular elements tend to represent the deformation of corners better than the quadratic elements. To explore the stress analysis further, the simulation was carried out using the 3D analysis.

4.1.2 Mesh Sensitivity Analysis

A sensitivity analysis was done to determine the appropriate size and shape of elements to use. The model in Figure 16 shows the dimensions of the part and the stress key for the stress distribution within the part in MPa.

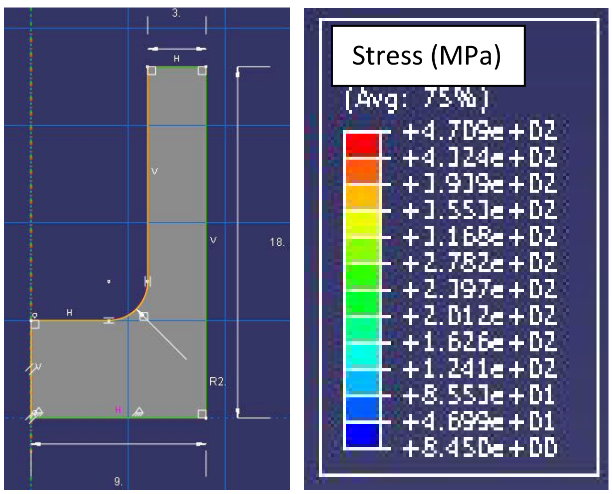

Figure 16: Dimensions and stress scale

Different simulation were done to analyse the effects of changing the element size on the the results obtained from the finite element simulation. Figure 17 shows the comparison between two different mesh sizes.

	Small Mesh Size	Large Mesh Size
Compaction	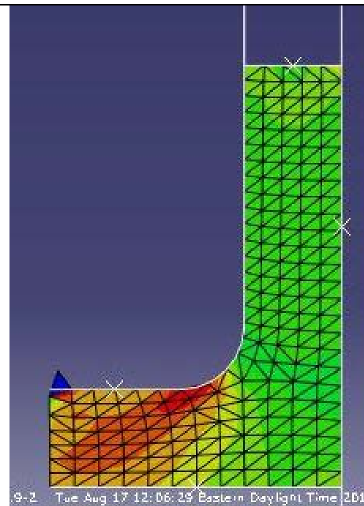	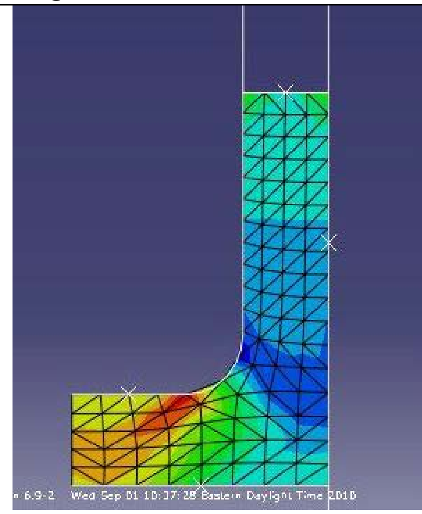
Unload	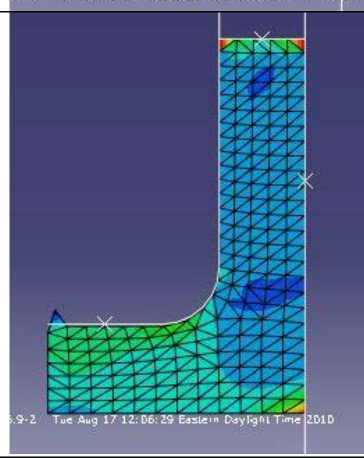	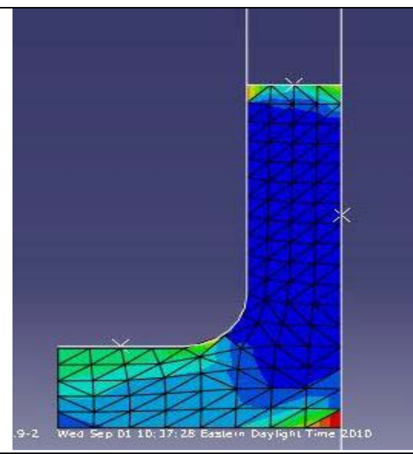
Ejection	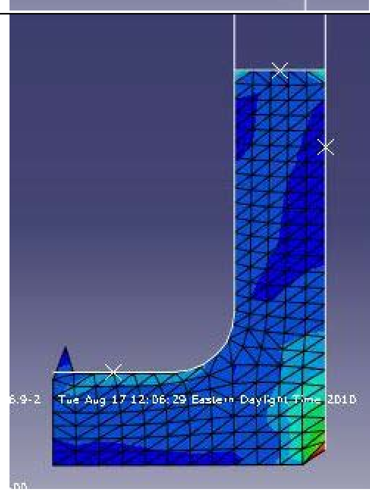	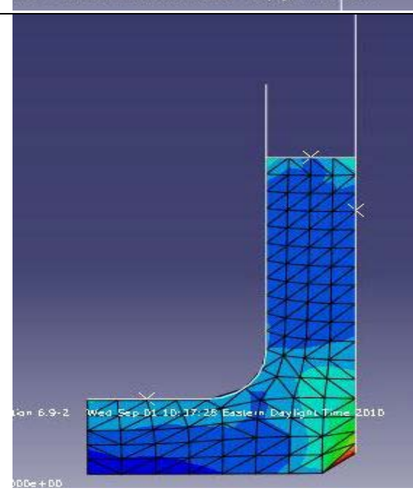

Figure 17: Mesh Sensitivity Analysis

In the simulation, the student version of ABAQUS was utilized for the analysis of the various steps involved in a simple cup model compaction. There are several limitations of the software, some of which include the limited mesh size (1000 nodes); and the availability of some parameters and analysis options were limited. This resulted in the failed ejection as shown in the ejection phase in Figure 17.

4.1.3 Elements Type

The element control used in the simulation was explicit, and the element used was a 3-node axisymetric triangle. The element shape used in this simulation was triangular because it was the shape that could adapt to the corners of the part model. Figure 18 shows that there is a difference in stress distribution of the same part when the element is changed between quadratic and triangular shapes while leaving all other factors the same. From this analysis it seems that the triangular element produced a smoother result for the cup model.

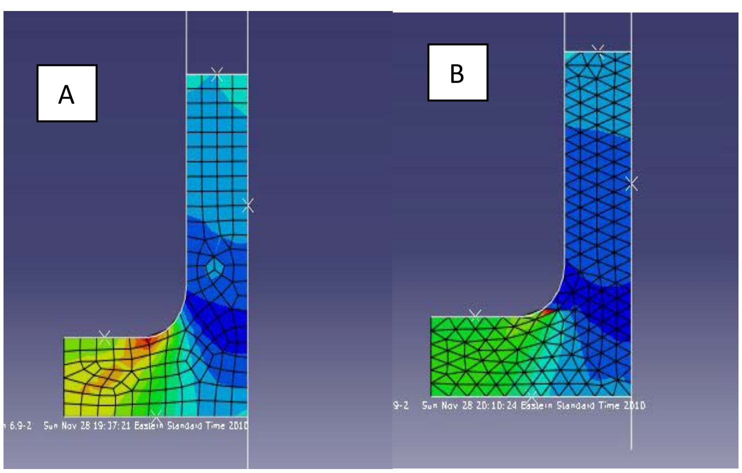

Figure 18: Quadratic shape element compared with triangular shape element (A: 4-node bilinear axisymmetric quadrilateral, B: 3-node axisymetric triangle

4.1.4 3D model

In the 3D models, the dimensions and properties were kept similar to that of the axisymmetric model. This method made it possible to see the stress distributions throughout the cylindrical cup through the use of section views which were not available in the axisymmetric model. The diagrams in Figure 19 and Figure 20 show the section views through the compaction and ejection phases.

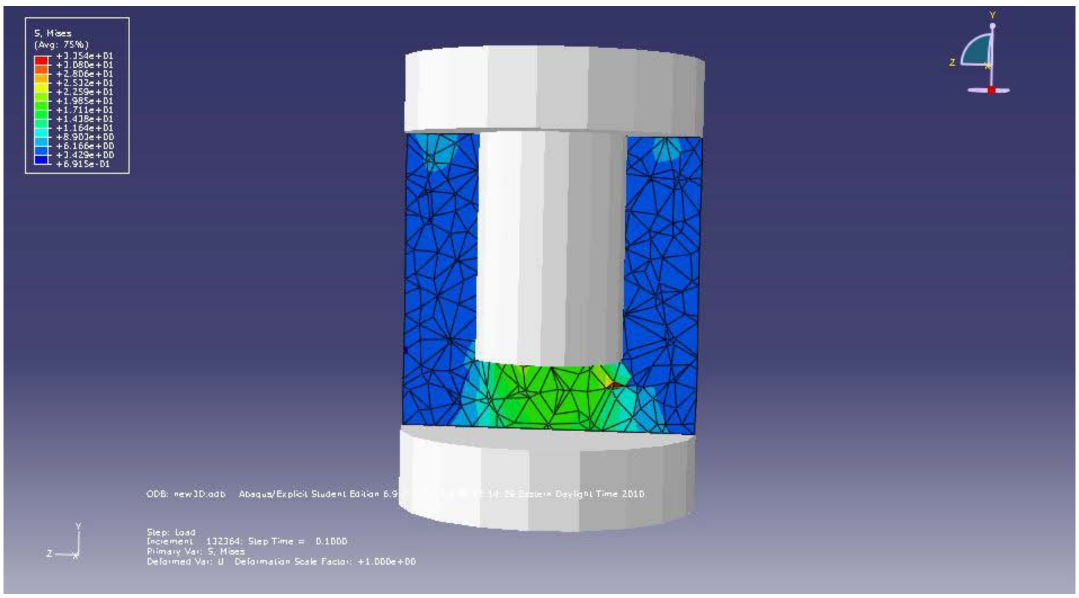

Figure 19: Compaction of three dimensional cup model

After the compaction of the Cup, the Center rod and the top punch were removed, and the part was ejected using the bottom punch.

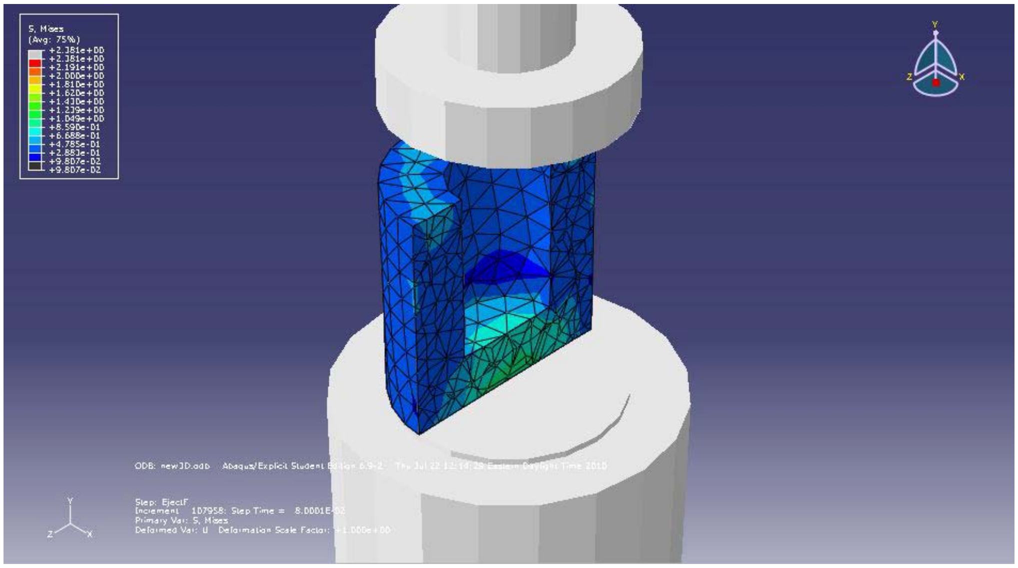

Figure 20: Ejected three dimensional cup model

When using the 3D modeling, the part was ejected without any errors. The stress distribution in the 3D analyses is similar to the axisymmetric simulation with stress concentration in the inner corners.

4.2 Rectangular Block Model

The second model attempted was a rectangular part. Figure 11 shows the loading schematic of the compaction process.

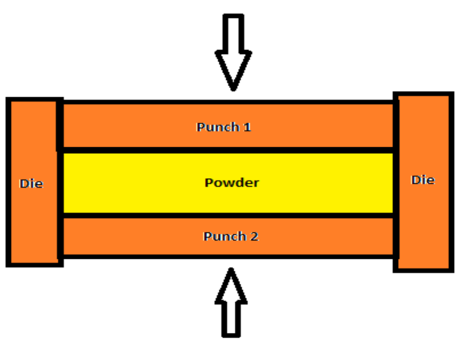

Figure 21: Schematic of Compaction Process

The 3D model was done in three steps: compaction, unloading, and the ejection phase. The important stages in this process were the compaction and ejection phases which are represented in Figure 22 and Figure 23, respectively.

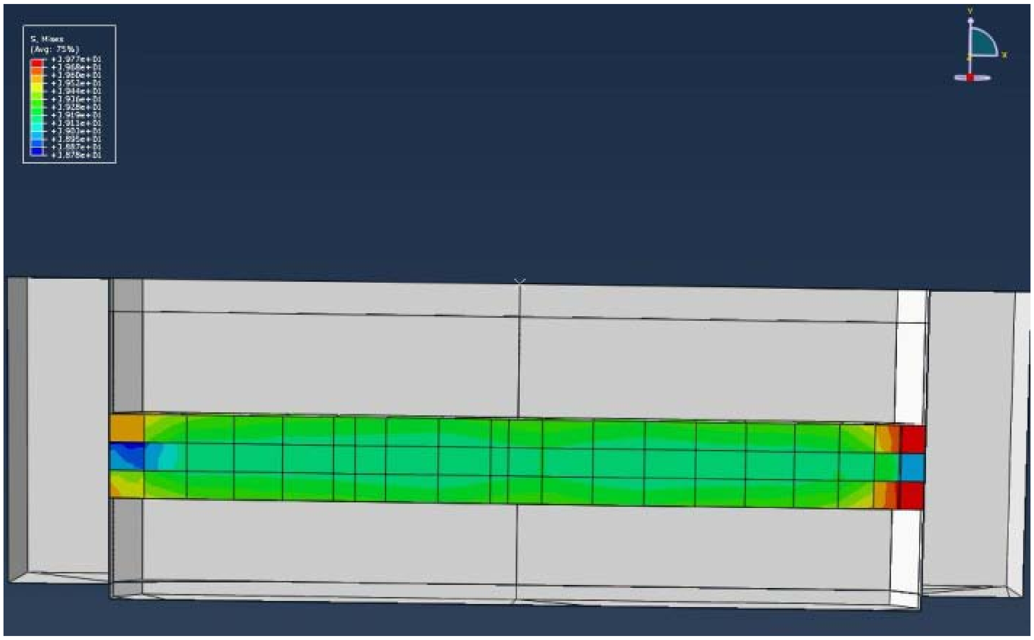

Figure 22: Rectangular block compaction

After the compaction, the part was the ejected by the removal of the top punch followed by using the bottom punch to eject the part by pushing it upward out of the die as shown in Figure 23.

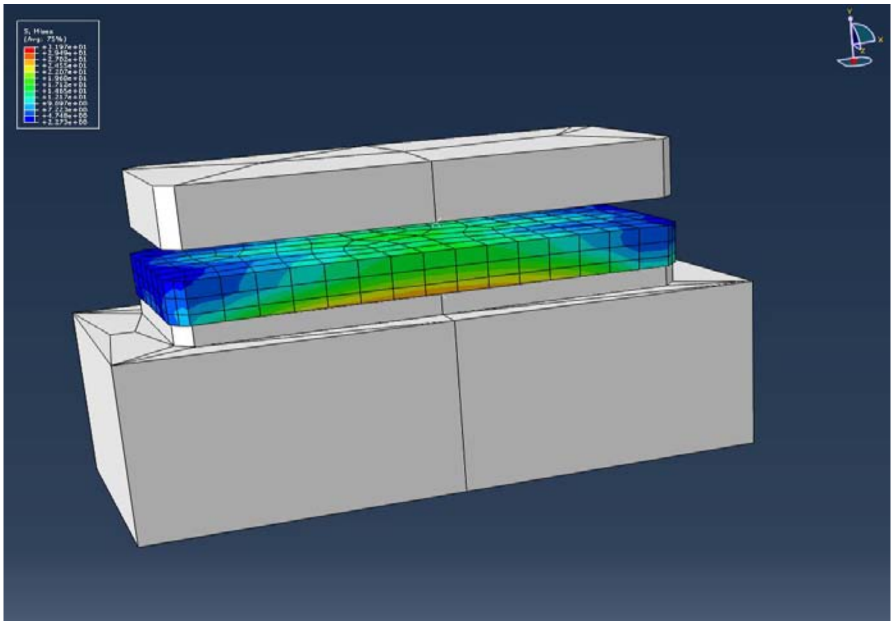

Figure 23: Ejected rectangular block

The results obtained from the analysis in the 3D models, show the stress distribution in the block. The results show that the maximum stress concentration was on the outer surface and point of contact with the punch.

In the ejection analysis different porosities were simulated and are tabulated below

Table 4: Maximum ejection stresses in MPa

Relative Porosity (%)	Ejection stress (MPa)
41.684	20
33.48	21.8
24.926	26.5
17.892	28
10.966	32

As expected, the ejection stresses increases as the relative porosity decreases (higher density).

4.2.1 Stress Distribution:

To further explore what happens within the compact, the images of several layers are portrayed in Figure 24 and Figure 25, which shows different stresses at different layers and porosities through the horizontal directions. The layers were at 20% dept, 50% dept and 80% dept from top to bottom.

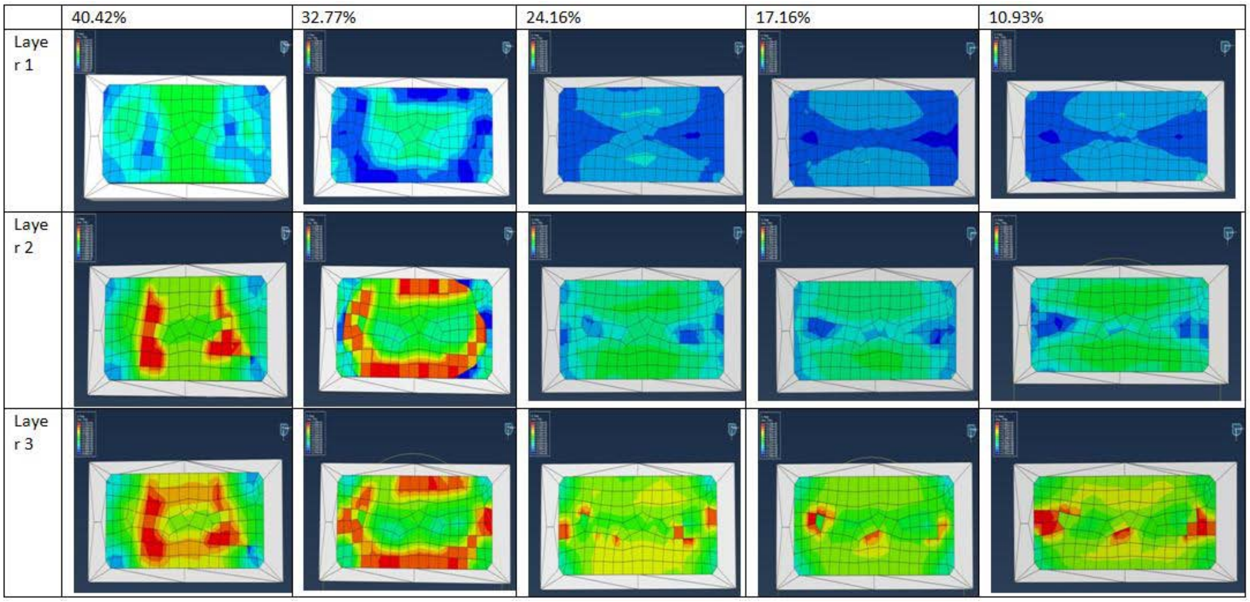

Figure 24: Relative Porosities and stress distribution in different layers

The diagrams in Figure 24 show the maximum tensile stress distribution and concentration with different relative porosities. Although they all have similar distribution, the model with the maximum relative porosity (the first column 40.42%) shows more of a stress gradient. Layer 3 which is the one at the bottom of the figure has the maximum stresses, which is consistent in all the parts with different relative porosities. The maximum stresses for the lower relative porosities appear to be more concentrated than that of the higher relative porosities, this is because lower relative porosities means higher densities and to generate higher densities, the compaction pressure has to increase which results in increased stresses within the part. The stress patterns follow the shape of the die; this shows that the forces from the die walls affect the powder differently at different relative porosities. From Figure 25, the different mesh and element size shows that the smaller meshes result in a better representation of the stress distribution.

Relative Porosity	Mesh seed 1.7	Mesh seed 2	Mesh seed 2.5
34.82%	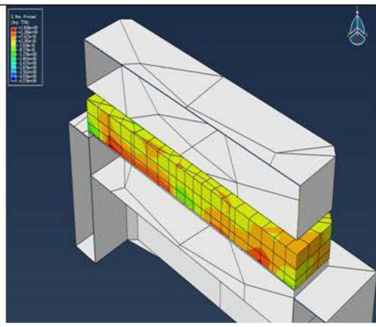	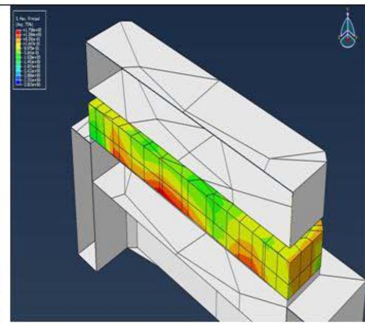	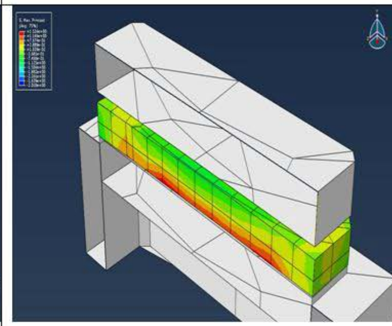

Figure 25: Relative porosity Mesh sizes

4.3 Gear Model

The last model to be simulated was a gear. Figure 26 and Figure 27 show the stress distribution during compaction and unloading of the gear.

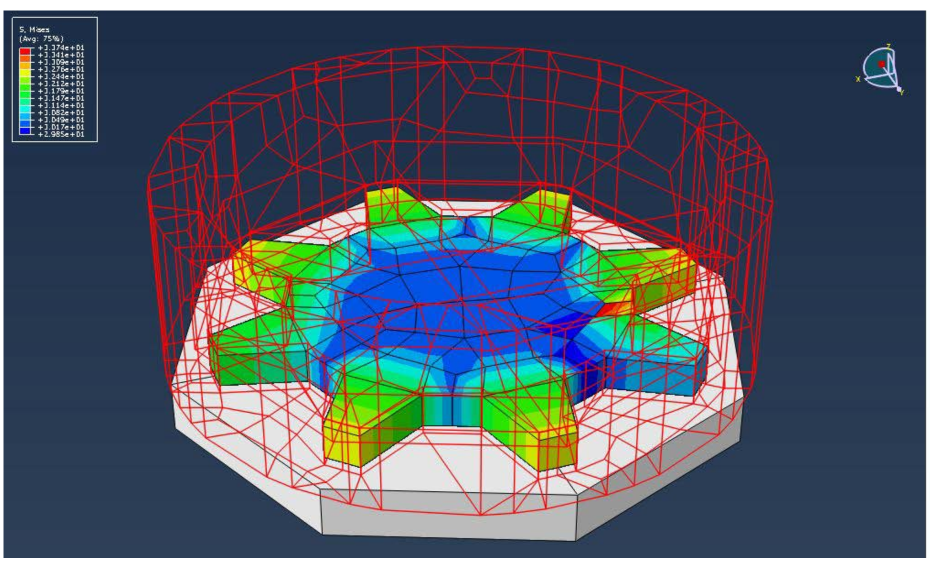

Figure 26: Gear in compaction stage

The gear model in Figure 26 shows results similar to previous models. During compaction, the maximum stresses are located in the gear teeth which are as expected since there is more surface contact on a smaller volume per teeth.

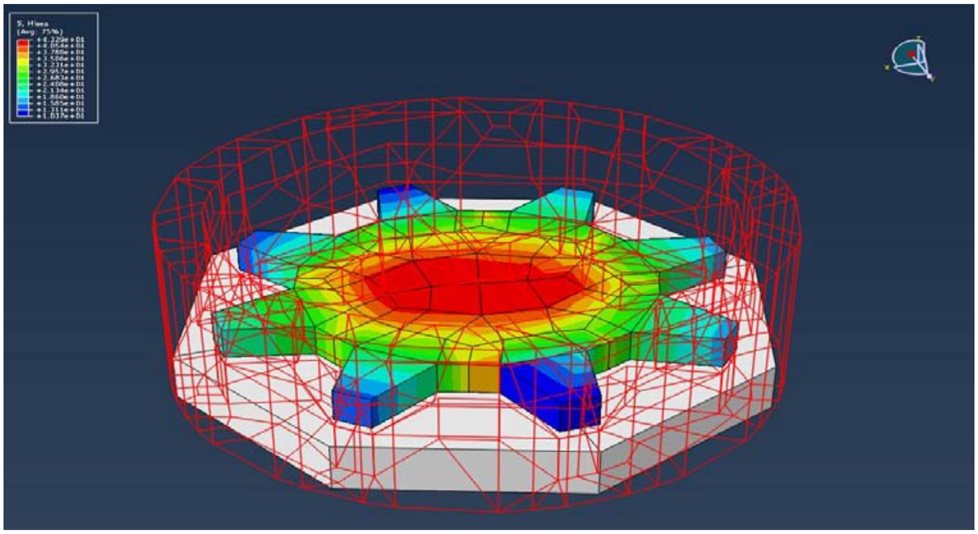

Figure 27: Gear Unloaded

During the unloading, there is a spring back effect which causes an increase in stresses at the center of the gear.

During the ejection and unloading phase, it can be noticed that some degree of spring-back occurs; this was noticed just as the part was ejected from the die, which caused an increase in stresses in the center of the gear. It was during this stage that fractures begin to form. In practice, to minimize the spring back the ejection and unloading are done in different stages, and in some instances there should be intermediate steps between unloading and ejection to help in minimizing the stress in the ejected part.

CHAPTER 5: SURVIVABILITY COMPUTATIONS

Using the survivability model in Equation 11, and the maximum stresses for 25 different models of each case study a survivability analysis was performed. This analysis is intended to compensate for uncertainties in FE modeling of the ejection stage and other important factors such as material properties, variation in powder size, etc. By using the statistical approach of survivability, some of these uncertainties can be mitigated.

5.1 Case Study 1: Rectangular Block

In this case study, the ejection stresses and strength of the prismatic part in Figure 28 was determined and analysed using the survivability model method established.

The production of the part was simulated and the maximum ejection stresses were extracted and compared with the strength of the part which was determined through the 3-point bend test.

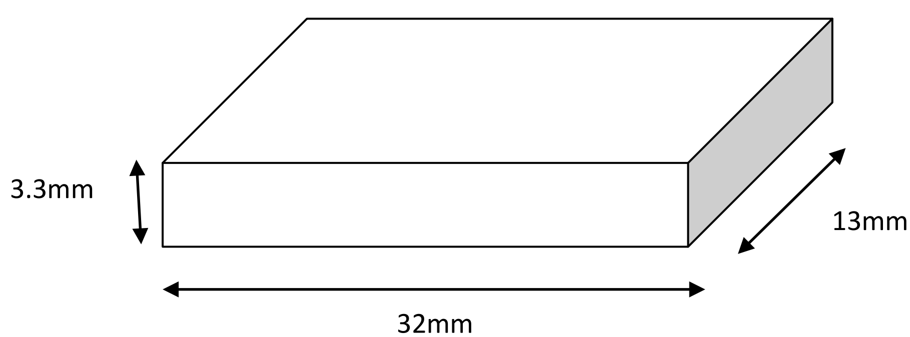

Figure 28: Dimensions of Prismatic Block

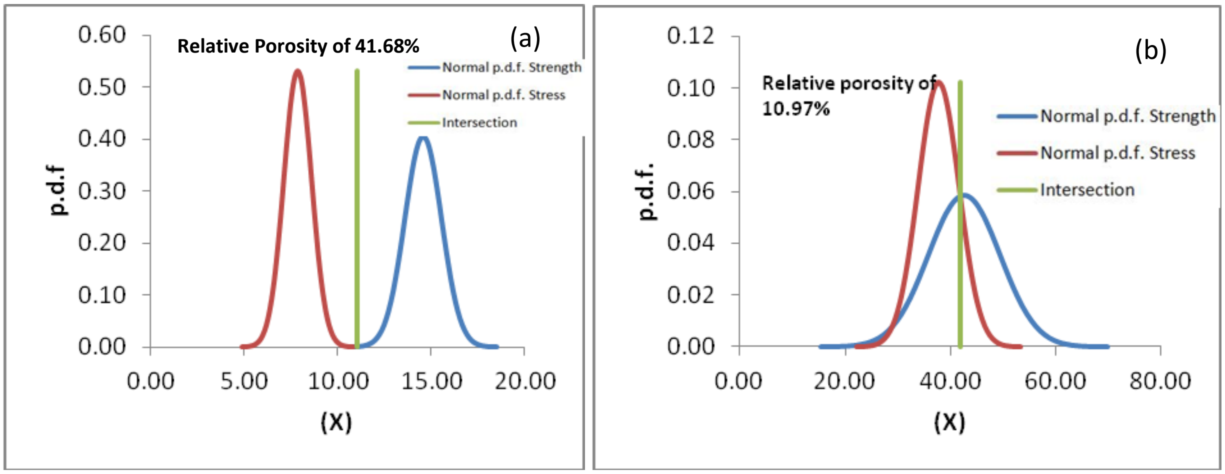

Figure 29: Normal distribution for survivability of part. Graph (a) is for a relative porosity of 41.68%, and graph (b) is for a relative porosity of 10.97%

Figure 29 shows the normal curves of the largest relative porosity of the block model. The curve on the left is for the normal distribution of stress in the ejected part, and the right represents the normal distribution of the maximum stress during the 3 point bend test. The normal curves are between relative porosities of 41.68% and 10.97%. The intersection shown in each of the graphs indicates the failure area, therefore the larger the intersected area, the lower the survivability of the part. The rest of the normal distribution graphs are shown in Appendix B.

Figure 30 shows the survivability graph for the rectangular block.

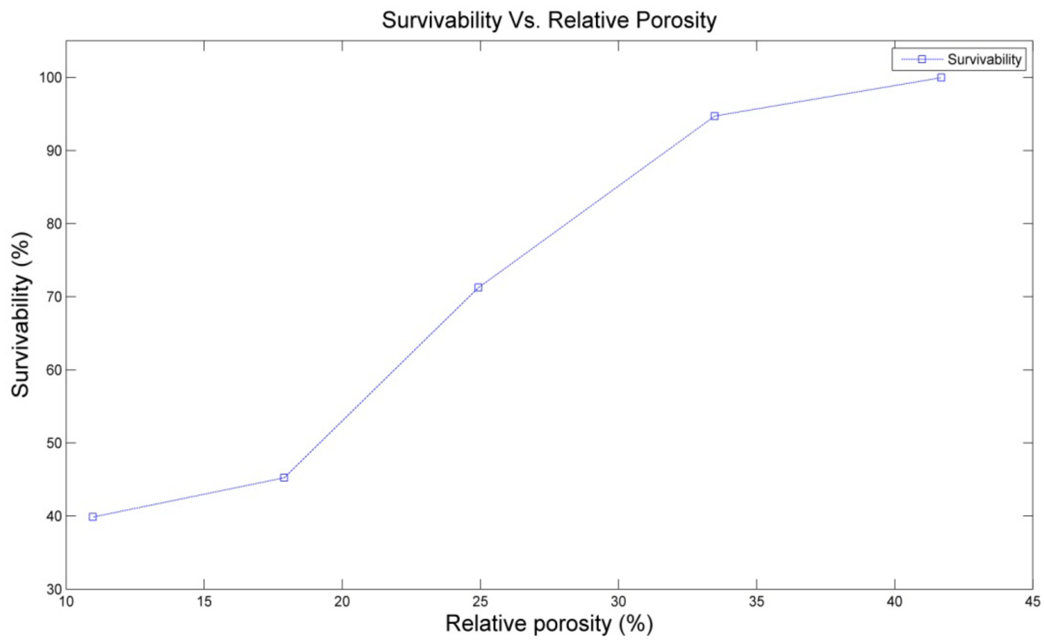

Figure 30: Survivability graph

According to Figure 30, the survivability of the part decreases as the relative porosity of the compact decreases. Although the lower relative porosities have higher strengths, the compacts with the higher relative porosities tend to have a higher chance of surviving the ejection process. The goal of this analysis is to be able to predict if a part of different shape or size, with the same material properties, would survive the ejection process.

5.2 Case Study 2: Bearing Model

As a second case study, the case of PM bearings was considered (see Figure 31). P/M bearings are in widespread use due to self lubricating and other beneficial attributes. Typically, these bearings have wall thicknesses of more than 1 mm and height to thickness ratio of between 2 to 4[3]. The process of compaction and ejection of these bearings were simulated using the calibrated FE model. The simulation was performed for a variety of relative densities.

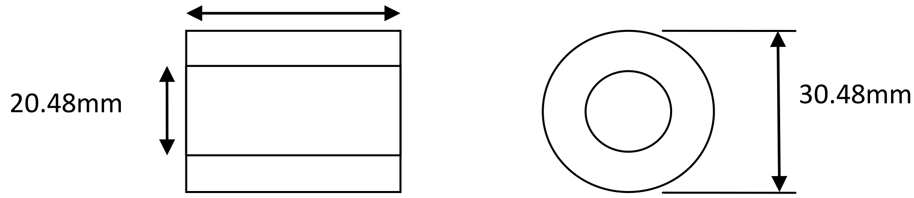

Figure 31: Schematic Representation of Journal Bearing Case Study

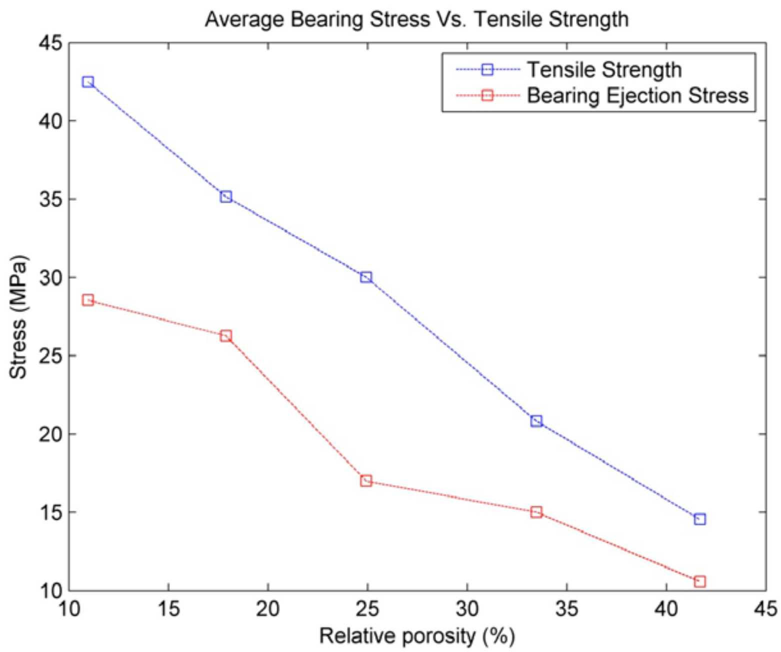

Figure 32: Average Ejection stresses of bearings compared with the tensile stresses obtained from the three point bend simulation

The graph in Figure 32 compares the maximum tensile stresses during the ejection of the bearing with the tensile strength obtained from the three point bend test of the simulation. From the graph, it can be observed that the ejection stresses of the bearings are below the tensile strength. The graph in Figure 33shows the survivability plot for the bearing model.

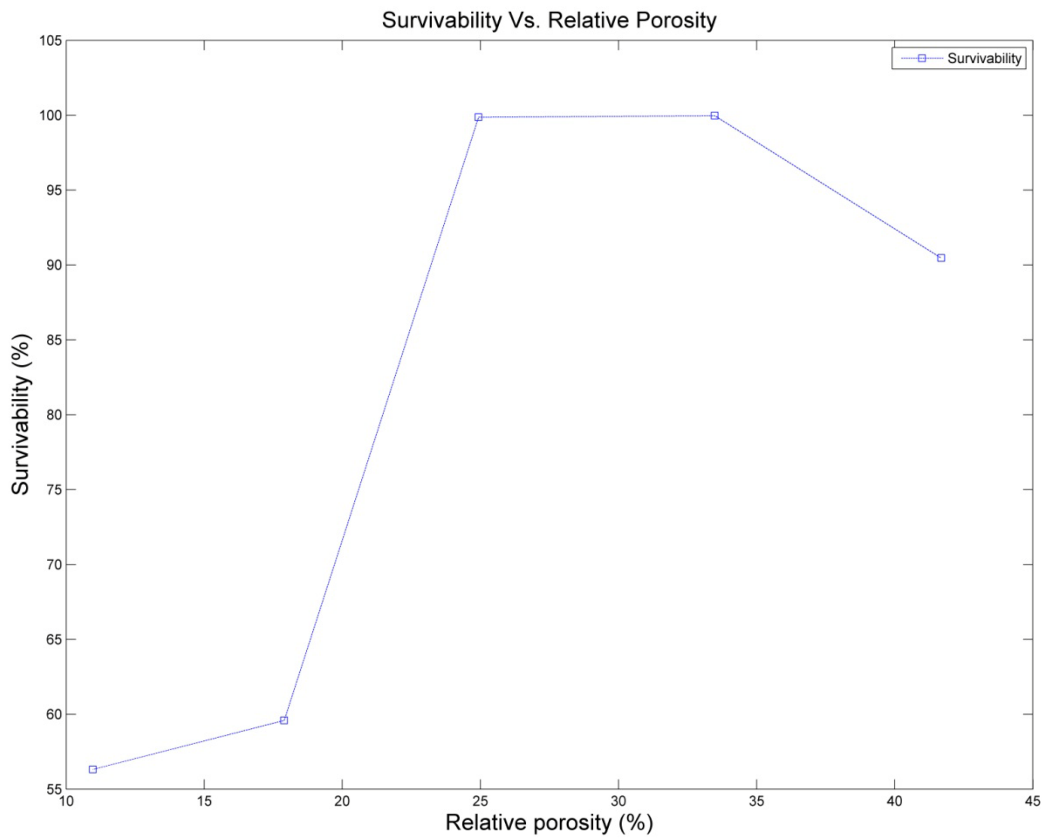

Figure 33: Survivability graph for bearing model

The survivability graph in Figure 33 for the bearing follows the pattern that predicts that the parts with higher relative porosity have a better chance of surviving the ejection process. The dip at the end of the graph could be caused by the approximation involved in the Drucker Prager Cap model when analysing powder as a continuous problem instead of as a discrete problem.

5.3 Case Study 3: Gear Model

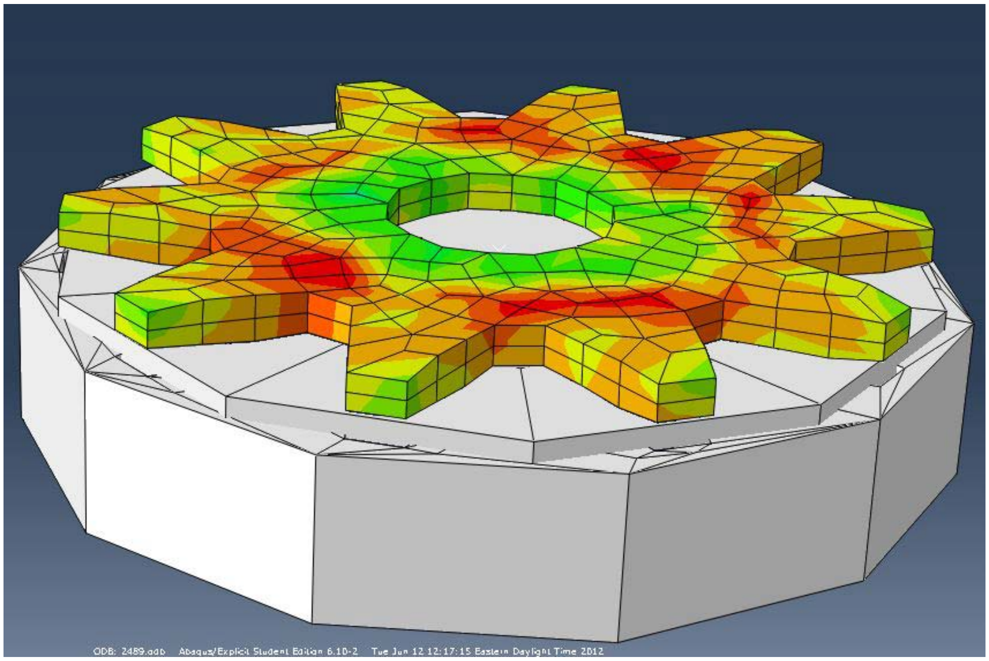

Figure 34: Gear model

As another case study the gear model shown in Figure 34 was used. The results in Figure 35 show that the ejection stresses in the gear would are very close to the tensile strength obtained from the three point bend simulation. This could be as a result of the complexity of the gear which could cause larger frictional stresses developed from the die walls and the powder part during ejection. It is expected that the friction between the die walls and the part would be marginally greater than that of the simple block model based on an increased surface area contact.

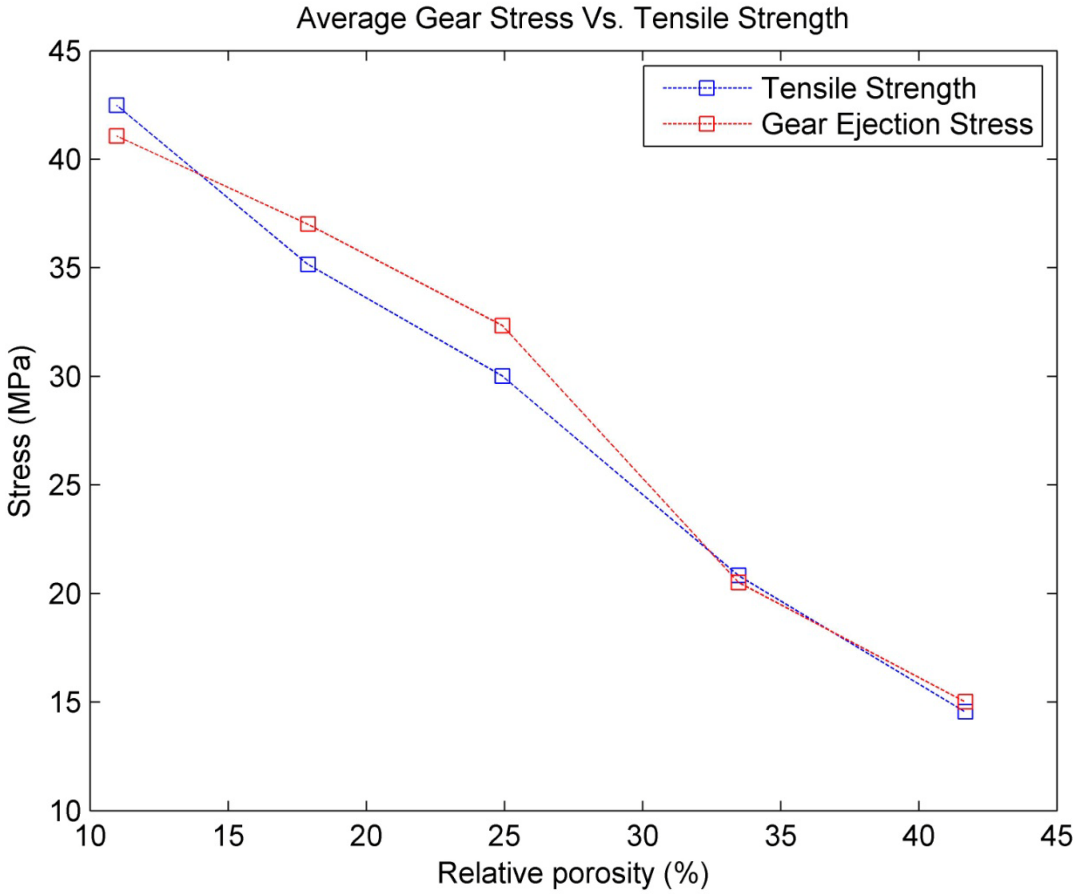

Figure 35: Relationship between the ejection stresses of gear and the tensile stresses.

According to the graph in Figure 35 the gear would fail during ejection based on the ejection system used and the different relative porosities. This can probably be prevented by using a different initial density (tap density) in the beginning of the compaction phase or changing the method of ejection. Another way would be to reduce the friction between the PM part and the die by changing the die material.

CHAPTER 6: CONCLUSION

The main focus of this work was to develop a methodology for determining the survivability of a powder metallurgy part during ejection using finite element analysis. All case studies were modeled using finite element method with the Drucker-Prager cap model. In PM controlling the relative porosity is a very important tool; it can be used in designing the right properties for the part being produced. A simple test was used for calibrating the Drucker-Prager model. Critical parameters were identified and a systematic approach for calibrating them was introduced.

Case studies involving various models were considered. The components simulated were general enough to make them applicable to several other components of similar complexities. The most important outcome was determining the survivability of the part after ejection. This was done by modeling similar parts with different relative porosities, and using survivability computations to analyse the changes in maximum stresses during ejection with relation to the strength of the ejected part.

The graphs obtained from the survivability computations show that although the parts with lower relative porosities have higher strengths, the parts with higher relative porosities have a higher chance of surviving the ejection process because the stresses generated during ejection are much less. Furthermore, the survivability computations show a wide range of values and can be used to predict more complex parts when trying to determine if a part will survive the ejection process based on the relative porosity and strength of the green compact after ejection. The results show that the relationship between the strength of the part and its ability to survive the ejection process is not proportional. Therefore, while developing process parameters for PM parts, interpolation from known successful set of parameters cannot be used.

6.1 Contributions

- A simple, effective method for calibrating FE models for modeling ejection, based on three point bending was developed.
- Statistical reliability calculations were used to mitigate the incomplete information and approximate nature of the FE modeling
- The feasibility of the procedure was shown using a number of case studies

6.2 Future Work

This work has the potential to be able to create a survivability index that can be used to determine if parts of different complexities and properties can be done successfully with powder metallurgy. In this work there was a limit to how sensitive the elements could be in the simulations which was restricted to 1000 nodes, it would be important to utilize more sensitive elements in the simulations for more precise results. Further research can be used to explore what a wider sample size to get more detailed results for the survivability model. It will also be important to explore what effects changing the die material would have on the PM part during the ejection process aimed at reducing friction between the die walls and the PM part.

APPENDIX A: STRESS VALUES

Table 5: Results of experiments at different compaction pressures

Nominal Compaction Pressure (MPa)	Sample No.	Actual Compaction Pressure (MPa)	Relative Porosity (%)	Tensile Failure Stress (MPa)
100	1	96	44.05	14.11
	2	99	42.41	14.57
	3	100	41.63	14.93
	4	102	40.42	15.74
	5	105	39.91	16.48
150	1	145	34.82	21.46
	2	147	34.24	21.74
	3	148	33.88	22.69
	4	151	32.77	22.75
	5	154	31.69	23.60
200	1	196	26.25	29.19
	2	200	25.31	29.82
	3	201	24.89	29.95
	4	203	24.16	30.43
	5	204	24.02	30.98
265	1	261	19.11	36.37
	2	263	18.31	37.14
	3	265	17.91	37.41
	4	266	17.16	37.55
	5	270	16.97	38.06
300	1	295	12.25	42.69
	2	298	11.64	43.71
	3	299	10.93	43.96
	4	300	10.54	44.12
	5	304	9.47	44.83

Table 6: Combination results showing comparison with experimental data

Relative Porosity %	Combination Count	Density	Cap Eccentricity	Angle of Friction	Material Cohesion	Max Stress	square difference	Experimental Max Stress
41.63%	1	3.15	0.3	35	0.3	26.74	139.48	14.93
	2	3.15	0.6	60	0.6	1.17	189.26	
	3	3.15	0.8	75	0.7	20.19	27.67	
	4	4.72	0.3	60	0.7	14.60	0.11	
	5	4.72	0.6	75	0.3	37.72	519.38	
	6	4.72	0.8	35	0.6	0.64	204.34	
	7	1.57	0.3	75	0.6	29.59	214.92	
	8	1.57	0.6	35	0.7	0.72	202.05	
	9	1.57	0.8	60	0.3	0.34	212.97	
33.88%	1	3.15	0.3	35	0.3	33.23	111.09	22.69
	2	3.15	0.6	60	0.6	1.50	449.10	
	3	3.15	0.8	75	0.7	13.12	91.58	
	4	4.72	0.3	60	0.8	22.09	0.36	
	5	4.72	0.6	75	0.3	17.97	22.28	
	6	4.72	0.8	35	0.6	0.60	487.76	
	7	1.57	0.3	75	0.6	33.52	117.29	
	8	1.57	0.6	35	0.7	0.95	472.78	
	9	1.57	0.8	60	0.3	1.33	819.28	
24.89%	1	3.15	0.3	35	0.3	13.96	76.21	29.95
	2	3.15	0.6	60	0.6	1.82	435.56	
	3	3.15	0.8	75	0.7	20.21	6.15	
	4	4.72	0.3	60	0.7	14.82	61.94	
	5	4.72	0.6	75	0.3	24.72	4.12	
	6	4.72	0.8	35	0.6	0.54	490.69	
	7	1.57	0.3	75	0.6	44.21	463.11	
	8	1.57	0.6	35	0.7	0.82	478.11	
	9	1.57	0.8	60	0.3	1.71	440.03	
17.91%	1	3.15	0.3	35	0.3	30.20	51.98	37.41
	2	3.15	0.6	60	0.6	1.16	1314.43	
	3	3.15	0.8	75	0.7	39.27	3.46	
	4	4.72	0.3	60	0.7	6.72	942.00	
	5	4.72	0.6	75	0.3	30.36	49.70	
	6	4.72	0.8	35	0.6	0.42	1367.99	
	7	1.57	0.3	75	0.6	58.27	435.14	
	8	1.57	0.6	35	0.7	0.42	1368.02	

	9	1.57	0.8	60	0.3	1.02	1323.94	
10.93%	1	3.15	0.3	35	0.3	2.92	1684.20	43.96
	2	3.15	0.6	60	0.6	1.22	1826.79	
	3	3.15	0.8	75	0.7	28.13	250.59	
	4	4.72	0.3	60	0.7	7.84	1305.02	
	5	4.72	0.6	75	0.3	37.04	47.89	
	6	4.72	0.8	35	0.6	0.12	1922.22	
	7	1.57	0.3	75	0.6	47.49	12.46	
	8	1.57	0.6	35	0.7	0.01	1931.91	
	9	1.57	0.8	60	0.3	2.05	1756.87	

Table 7: Maximum stress values

Relative Porosity (%)	Relative Density (%)	Experimental Results	Simulated Results	Ejected Results
		Stress (Mpa)	Stress (Mpa)	Stress (Mpa)
44.05	55.95	14.14	12.8	7.149
42.41	57.59	14.57	14.84	7.42
41.63	58.37	14.93	15.09	8.796
40.42	59.58	15.74	15.07	7.343
39.91	60.09	16.48	14.95	8.509
34.82	65.18	21.46	20.07	10.93
34.24	65.76	21.74	22.92	13.08
33.88	66.12	22.69	20.23	17.57
32.77	67.23	22.75	20.96	13.83
31.69	68.31	23.60	19.98	14.11
26.25	73.75	29.19	32.96	17.84
25.31	74.69	29.82	28.93	24.22
24.89	75.11	29.95	25.41	18.73
24.16	75.84	30.43	31.07	24.05
24.02	75.98	30.98	31.74	27.81
19.11	80.89	36.37	31.13	30.26
18.31	81.69	37.14	36.24	31.4
17.91	82.09	37.41	37.76	25.75
17.16	82.84	37.55	33.6	34.14

16.97	83.03	38.06	37.08	35.34
12.25	87.75	42.69	38.51	35.68
11.64	88.36	43.71	43.64	36.62
10.93	89.07	43.96	34.85	32.8
10.54	89.46	44.12	52.98	40.28
9.47	90.53	44.83	42.45	42.68

APPENDIX B: SURVIVABILITY GRAPHS

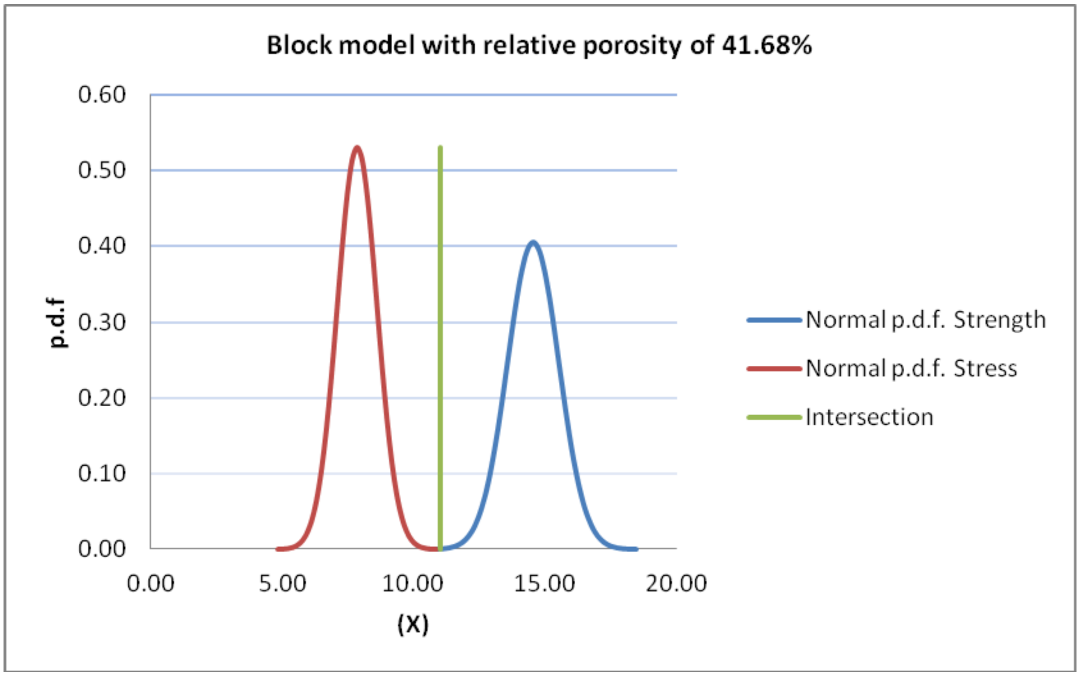

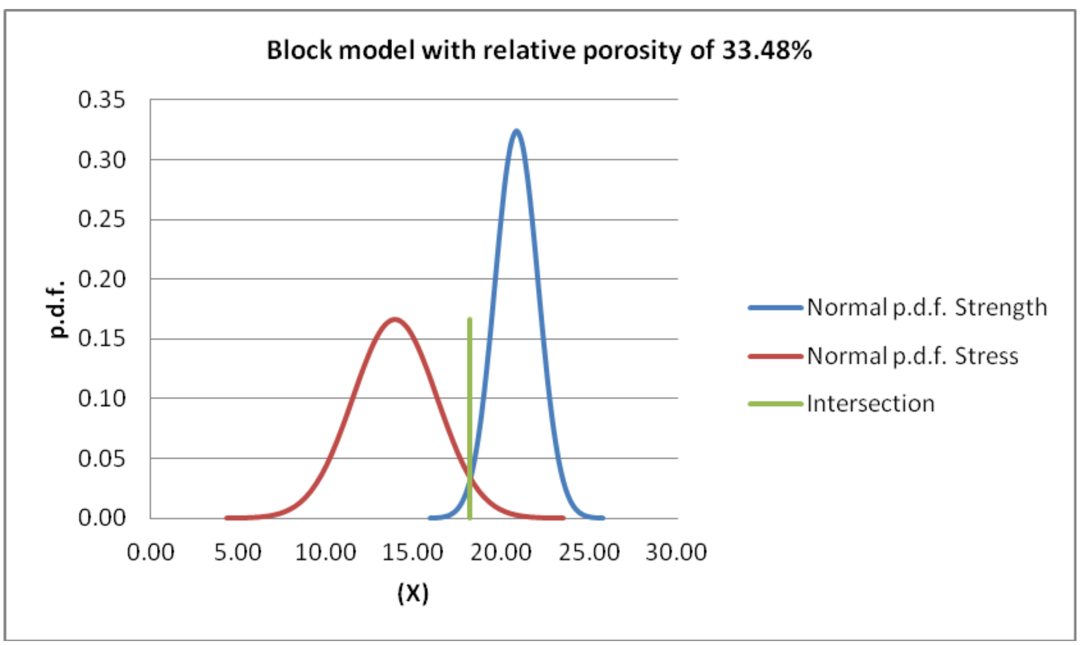

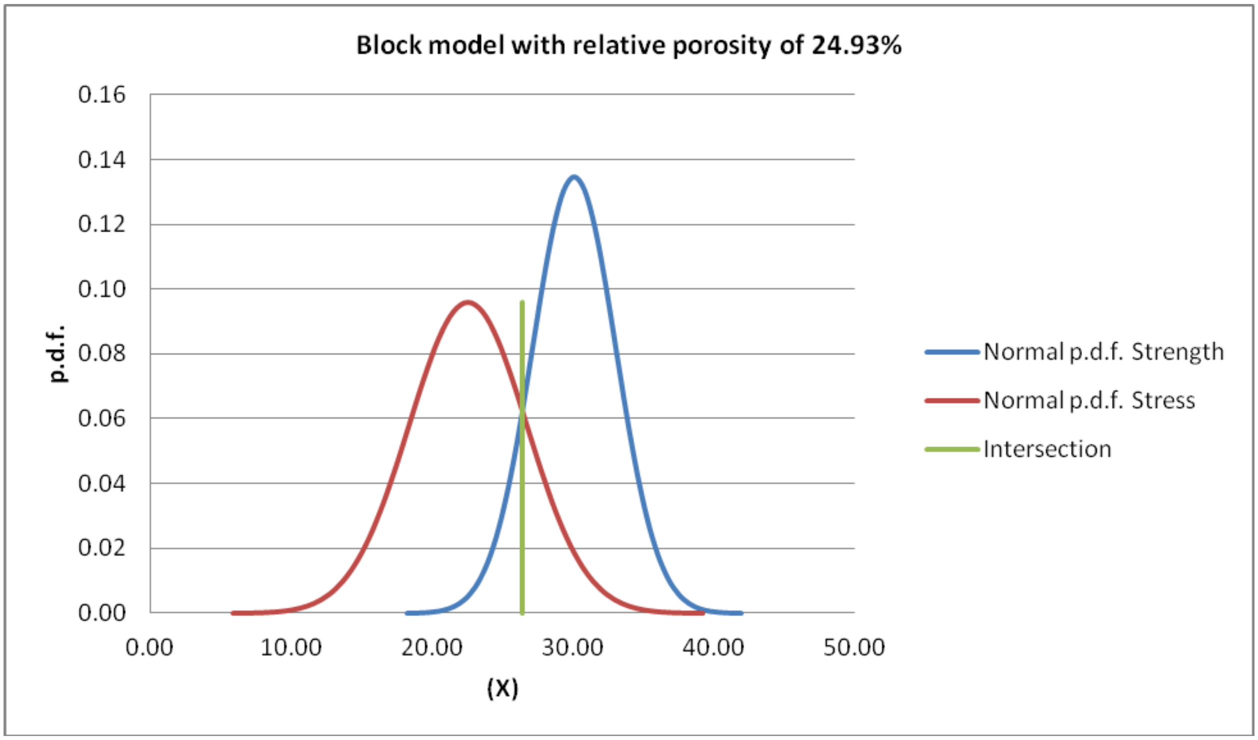

Block model with relative porosity of 24.93%
0.16
0.14
0.12
0.10
0.08
0.06
0.04
0.02
0.00
p.d.f.
0.00
10.00
20.00
30.00
40.00
50.00
(X)
Normal p.d.f. Strength
Normal p.d.f. Stress
Intersection

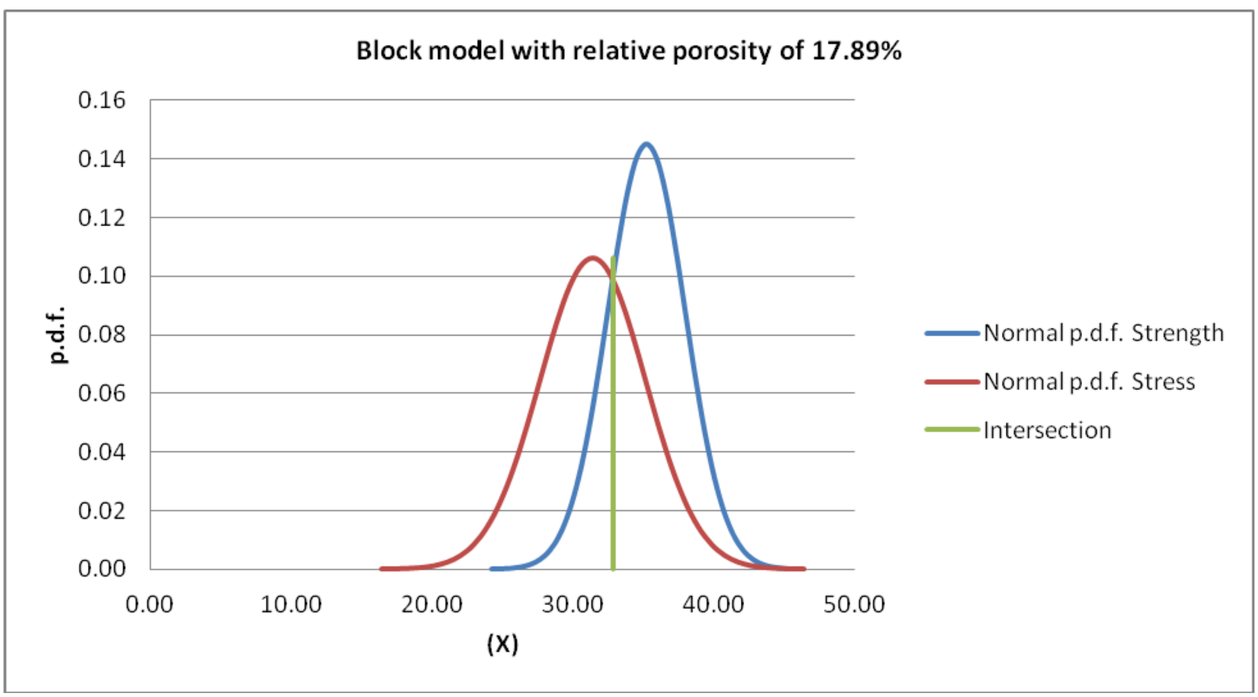

Block model with relative porosity of 17.89%
0.16
0.14
0.12
0.10
0.08
0.06
0.04
0.02
0.00
p.d.f.
0.00
10.00
20.00
30.00
40.00
50.00
(X)
Normal p.d.f. Strength
Normal p.d.f. Stress
Intersection

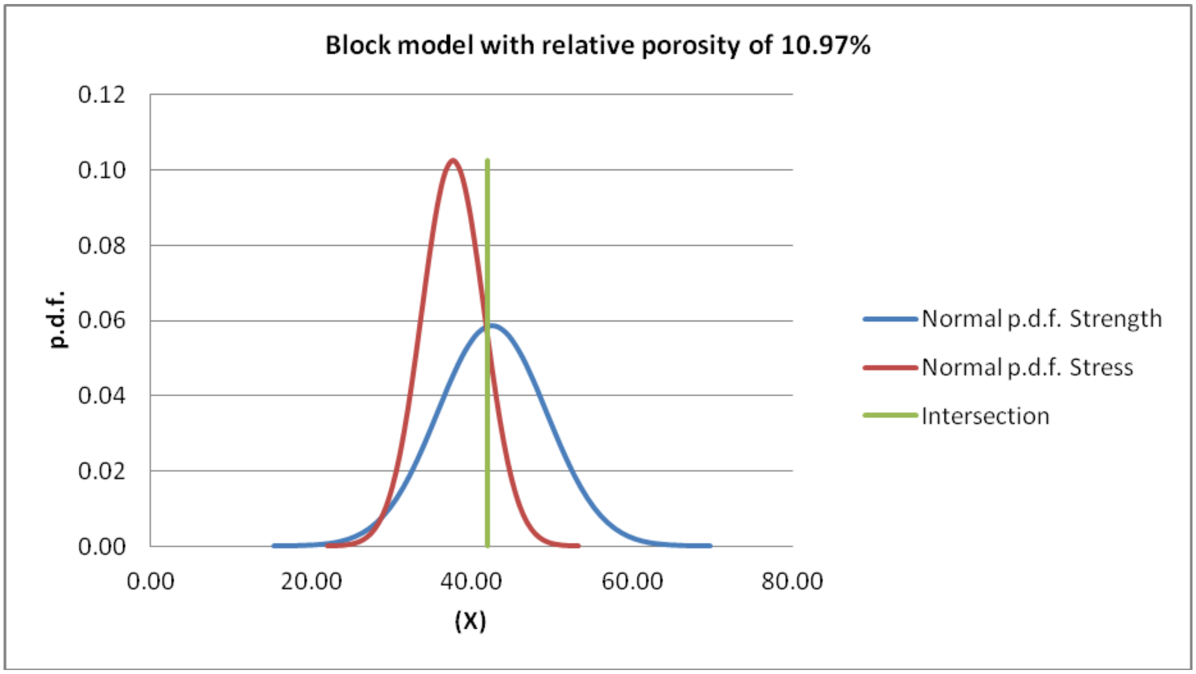
Block model with relative porosity of 10.97%
p.d.f.
0.12
0.10
0.08
0.06
0.04
0.02
0.00
0.00
20.00
40.00
60.00
80.00
(X)
Normal p.d.f. Strength
Normal p.d.f. Stress
Intersection

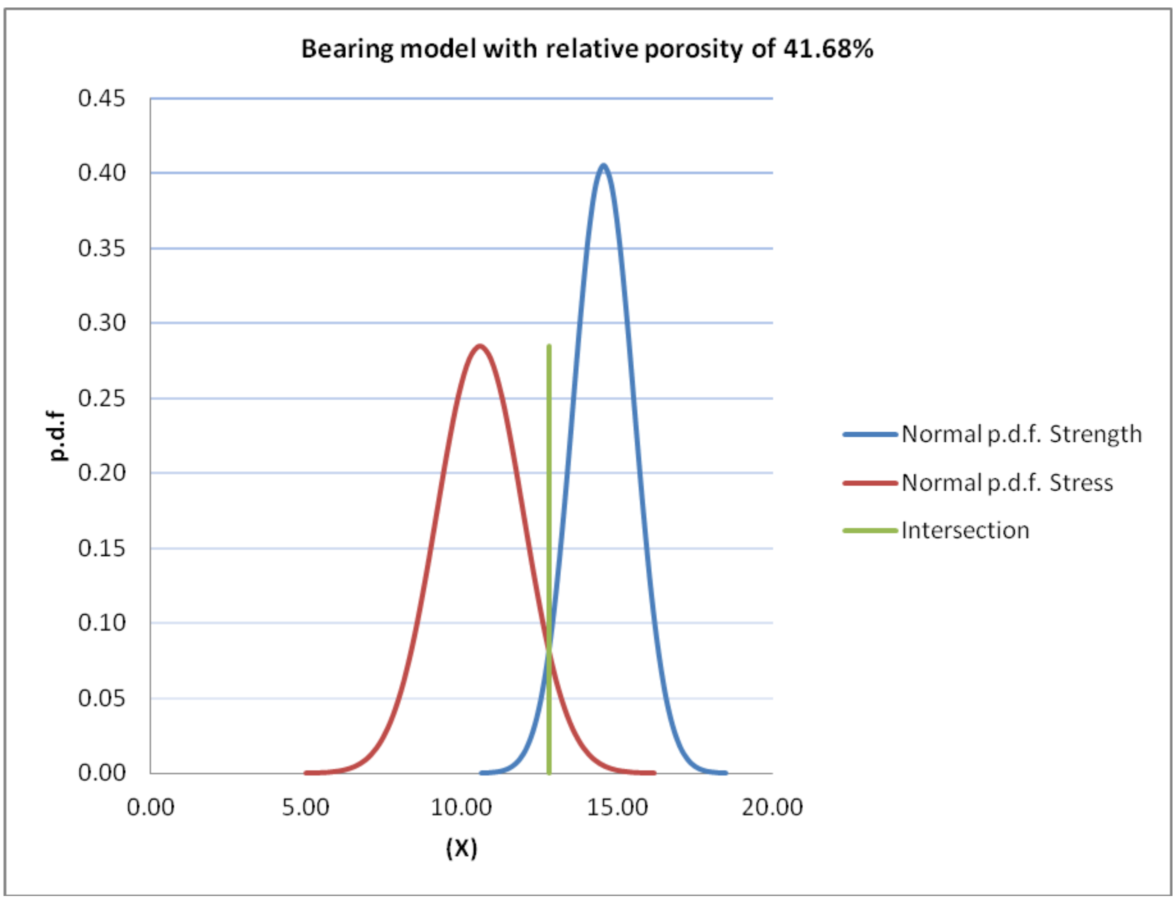
Bearing model with relative porosity of 41.68%
p.d.f
0.45
0.40
0.35
0.30
0.25
0.20
0.15
0.10
0.05
0.00
0.00
5.00
10.00
15.00
20.00
(X)
Normal p.d.f. Strength
Normal p.d.f. Stress
Intersection

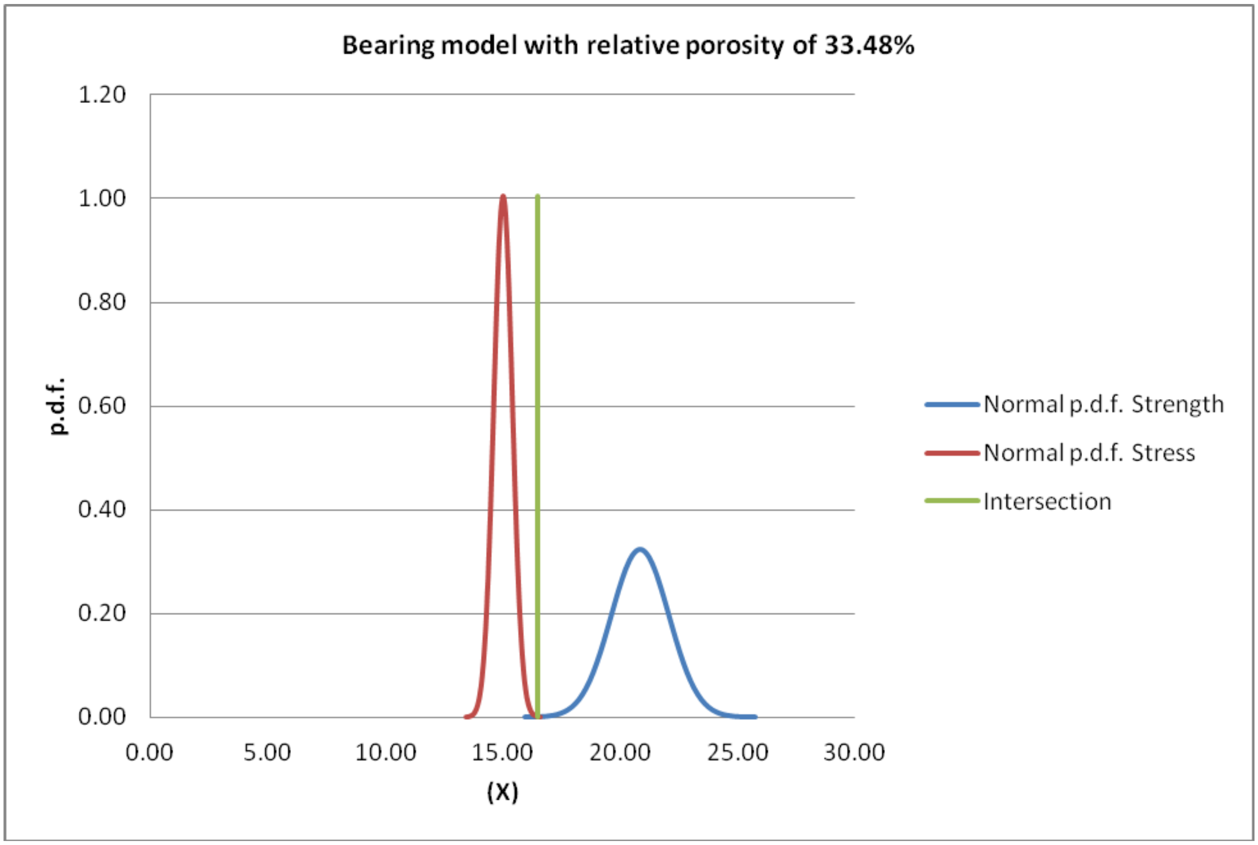
Bearing model with relative porosity of 33.48%
1.20
1.00
0.80
0.60
0.40
0.20
0.00
p.d.f.
0.00
5.00
10.00
15.00
20.00
25.00
30.00
(X)
Normal p.d.f. Strength
Normal p.d.f. Stress
Intersection

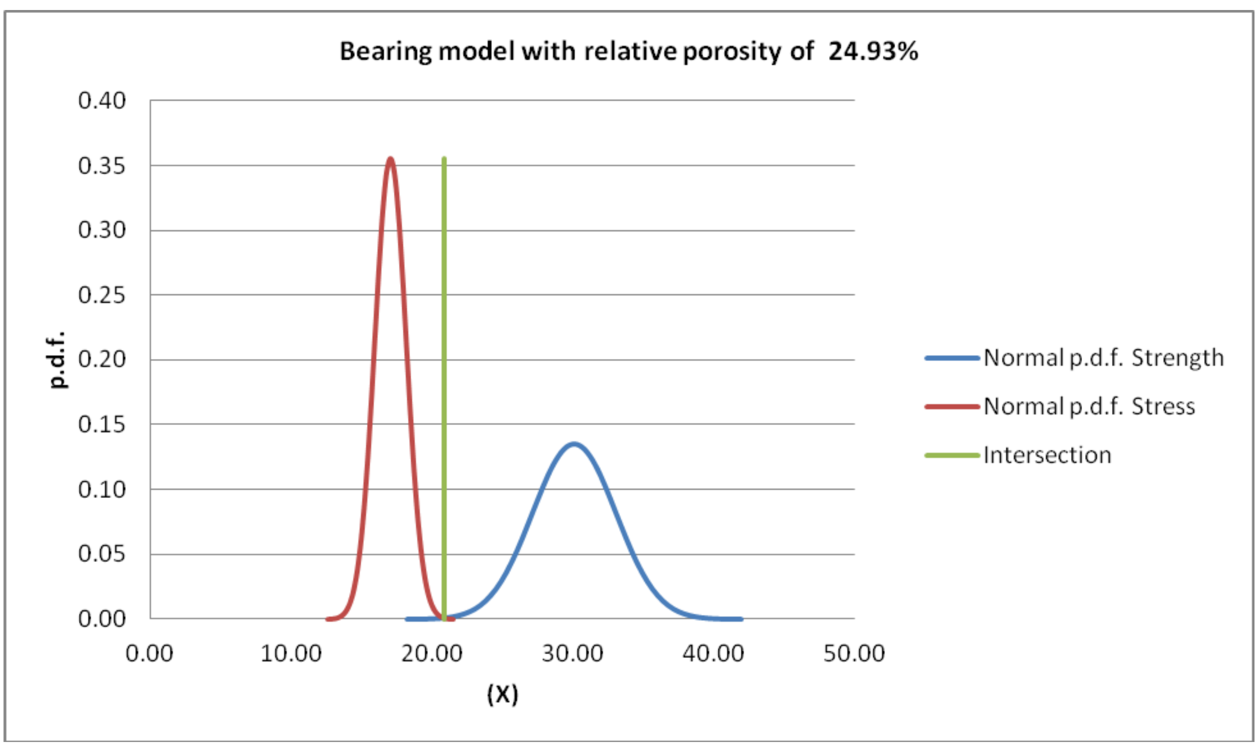
Bearing model with relative porosity of 24.93%
0.40
0.35
0.30
0.25
0.20
0.15
0.10
0.05
0.00
p.d.f.
0.00
10.00
20.00
30.00
40.00
50.00
(X)
Normal p.d.f. Strength
Normal p.d.f. Stress
Intersection

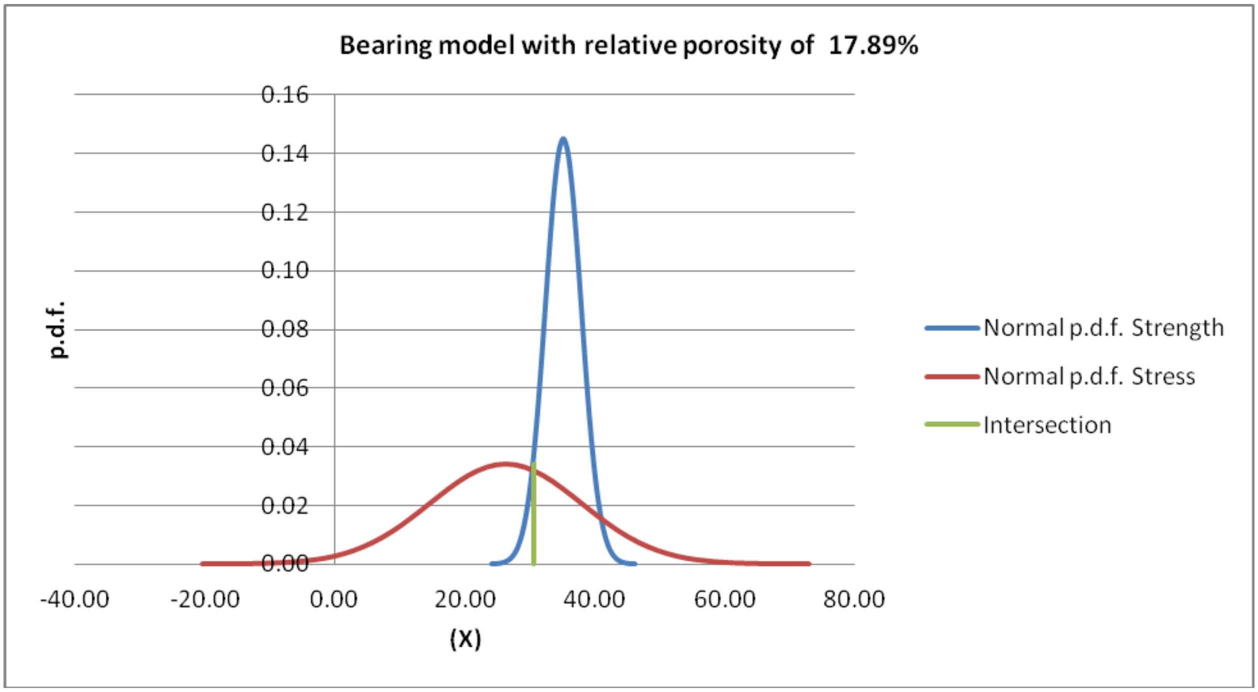
Bearing model with relative porosity of 17.89%
p.d.f.
0.16
0.14
0.12
0.10
0.08
0.06
0.04
0.02
0.00
-40.00
-20.00
0.00
20.00
40.00
60.00
80.00
(X)
Normal p.d.f. Strength
Normal p.d.f. Stress
Intersection

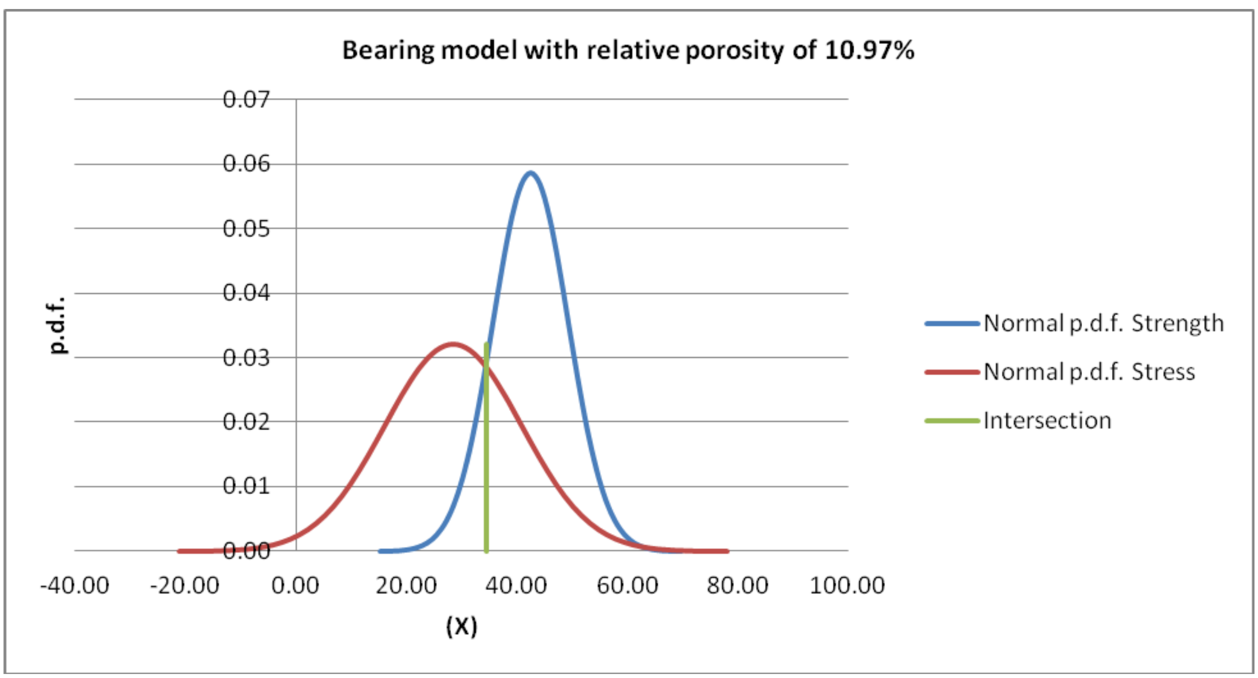
Bearing model with relative porosity of 10.97%
p.d.f.
0.07
0.06
0.05
0.04
0.03
0.02
0.01
0.00
-40.00
-20.00
0.00
20.00
40.00
60.00
80.00
100.00
(X)
Normal p.d.f. Strength
Normal p.d.f. Stress
Intersection

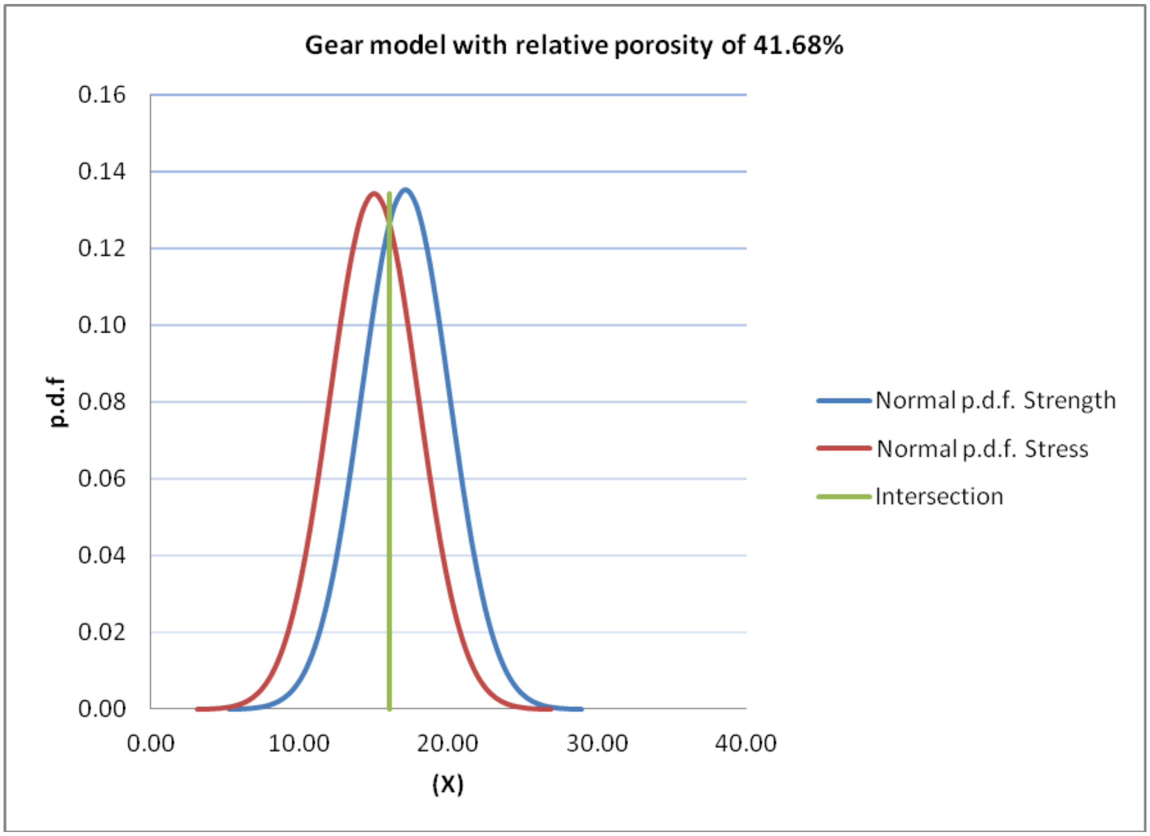
Gear model with relative porosity of 41.68%
0.16
0.14
0.12
0.10
0.08
0.06
0.04
0.02
0.00
p.d.f
0.00
10.00
20.00
30.00
40.00
(X)
Normal p.d.f. Strength
Normal p.d.f. Stress
Intersection

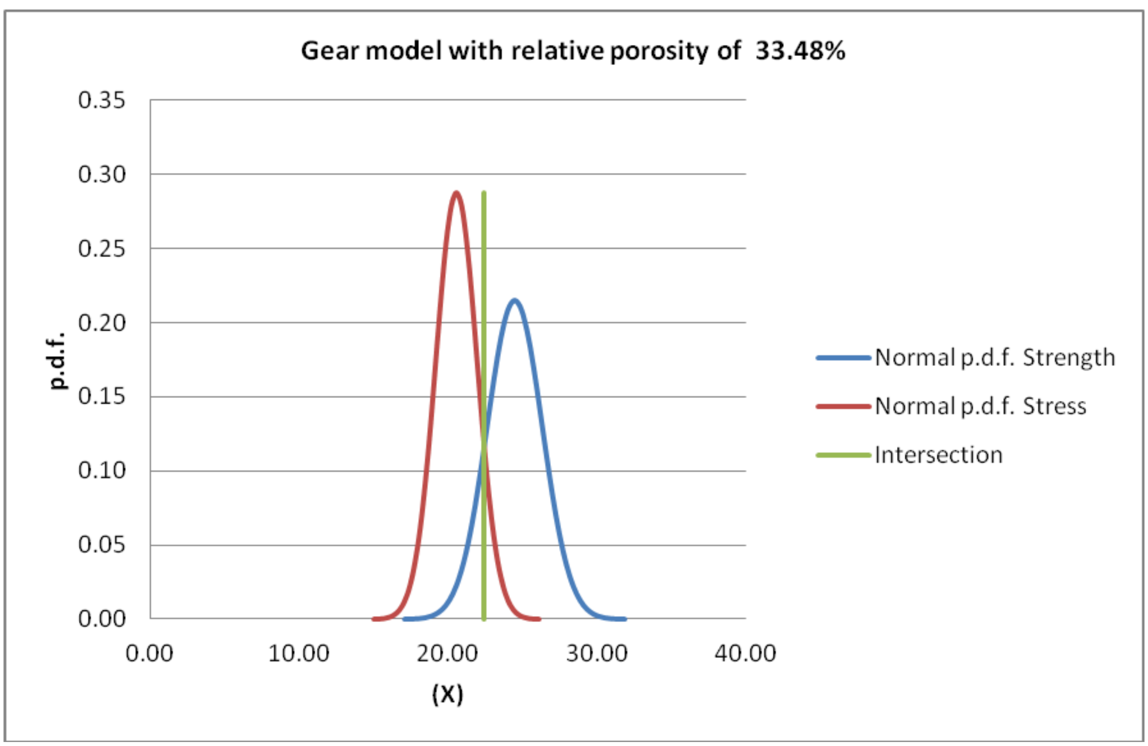
Gear model with relative porosity of 33.48%
0.35
0.30
0.25
0.20
0.15
0.10
0.05
0.00
p.d.f.
0.00
10.00
20.00
30.00
40.00
(X)
Normal p.d.f. Strength
Normal p.d.f. Stress
Intersection

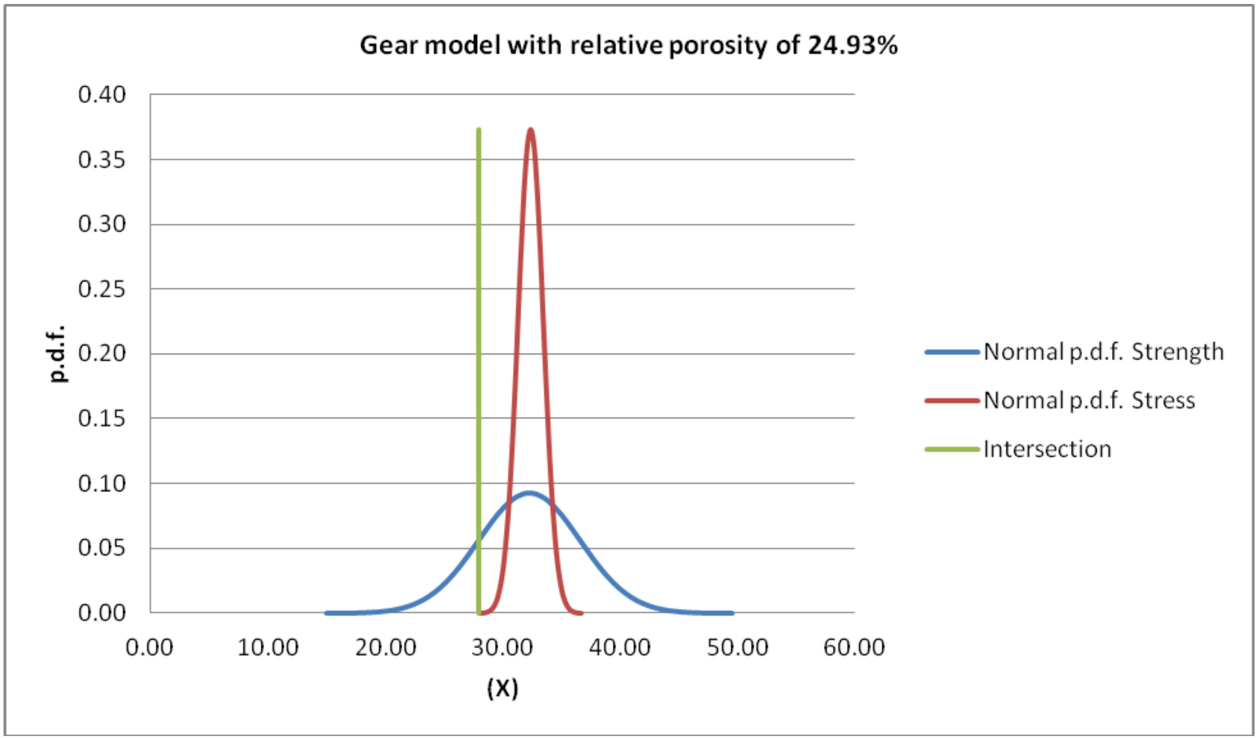
Gear model with relative porosity of 24.93%
0.40
0.35
0.30
0.25
0.20
0.15
0.10
0.05
0.00
p.d.f.
0.00
10.00
20.00
30.00
40.00
50.00
60.00
(X)
Normal p.d.f. Strength
Normal p.d.f. Stress
Intersection

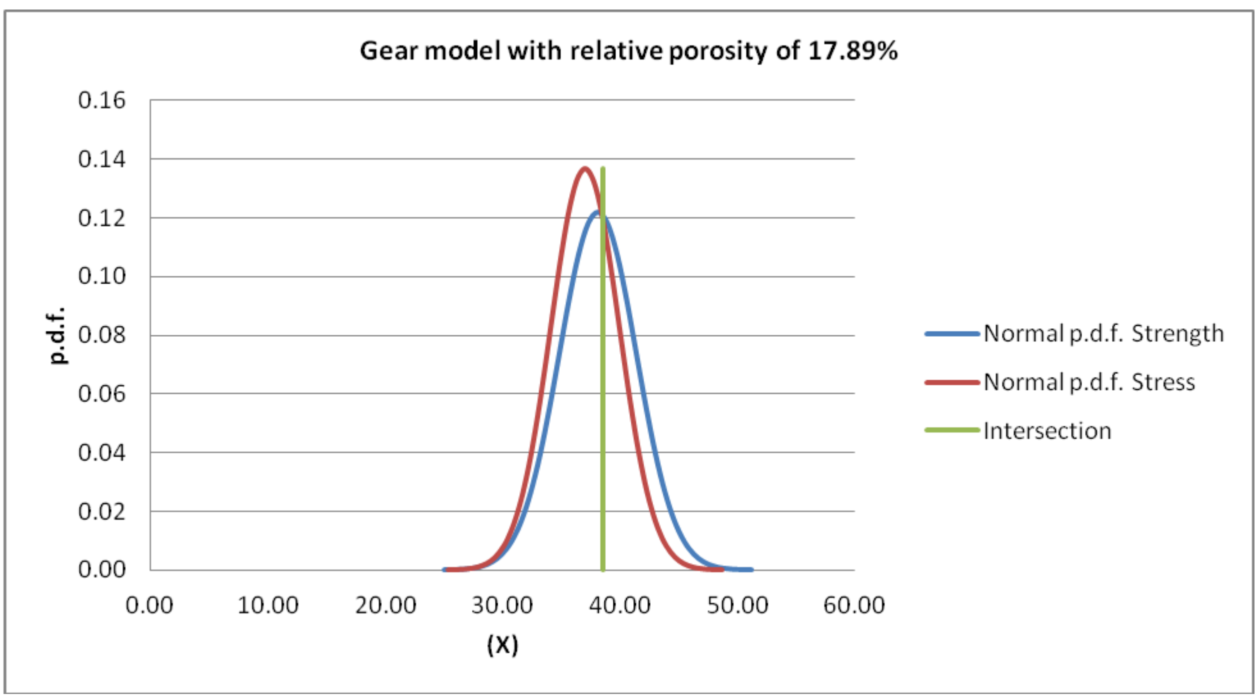
Gear model with relative porosity of 17.89%
0.16
0.14
0.12
0.10
0.08
0.06
0.04
0.02
0.00
p.d.f.
0.00
10.00
20.00
30.00
40.00
50.00
60.00
(X)
Normal p.d.f. Strength
Normal p.d.f. Stress
Intersection

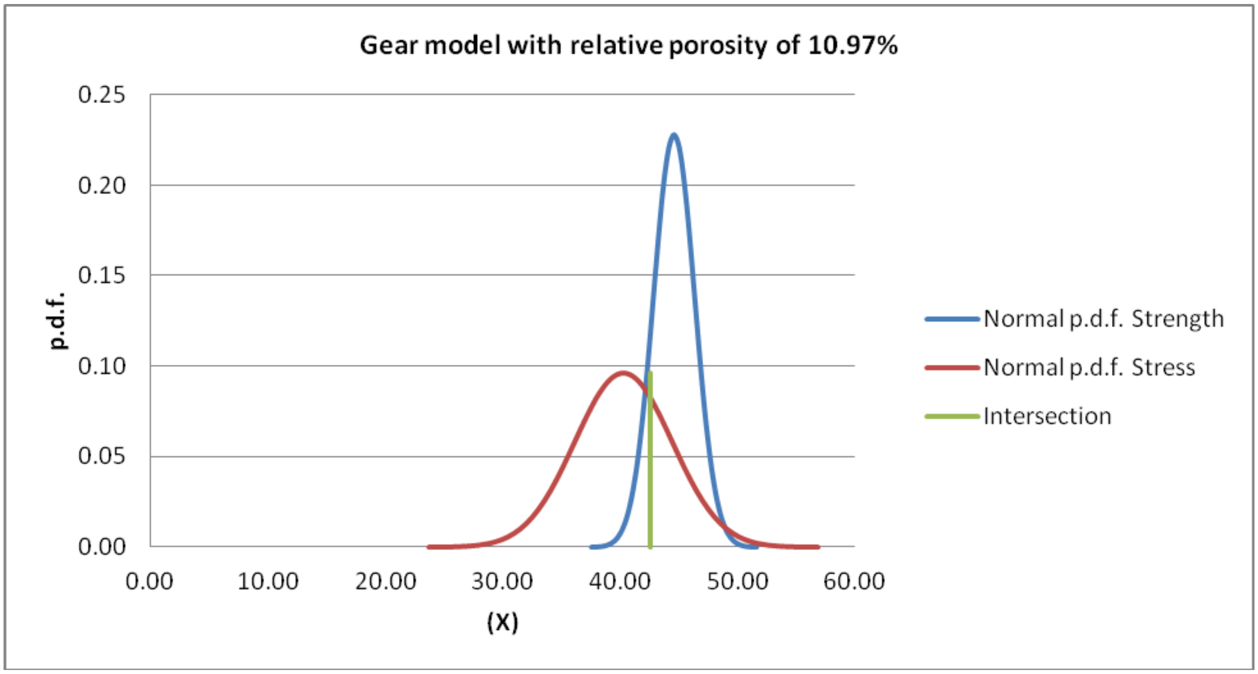
Gear model with relative porosity of 10.97%
0.25
0.20
0.15
0.10
0.05
0.00
p.d.f.
0.00
10.00
20.00
30.00
40.00
50.00
60.00
(X)
Normal p.d.f. Strength
Normal p.d.f. Stress
Intersection

REFERENCES

[1] H. C. A. G. Meftah Hrairi, "Modeling the Powder Compaction Proecess Ising the Finite Element Method and Inverse Optimization," *Powder Metallurgy,* pp. 631-647, 26 February 2011.

[2] AZoM.com, "The A to Z of Materials," 14 May 2002. [Online]. Available: http://www.azom.com/article.aspx?ArticleID=1414. [Accessed 12 May 2012].

[3] J. A. Schey, Introduction to Manufacturing Processes, Waterloo: Thomas Casson, McGraw-Hill, 2000.

[4] R. Marvin and H. Arnljot, System Reliability Theory, Models, Statistical Methods, and Applications, New Jersey: Wiley Inter-Science, 2nd ed., 2004.

[5] I. DeWolf, "MEMS reliability," *Microelectronics Reliability ,* vol. 43, pp. 1047-1048, 2003.

[6] G. S. Upadhyaya, Powder Metallurgy Technology, Cambridge: CAMBRIDGE INTERNATIONAL SCIENCE PUBLISHING, 2002.

[7] L. Han, J. Elliott, A. Bentham, A. Mills, G. Anidon and B. Hancock, "A modefied Drucker-Prager Cap model for die compaction simulation of pharmaceuical powders," *International Journal of Solids and Structures,* pp. 3088-3106, 2008.

[8] A. Bejarano, M. Riera and J. Prado, "Simulation of the compaction process of a two-level powder metallurgical part," *Materials Processing Technology,* pp. 34-40, 2003.

[9] B. Sven, J. Par and H. Hans-Ake, "Experimental characterisation of CaCo3 powder mix for high-pressure compaction modelling," *Powder Technology,* vol. III, no. 203, pp. 198-205, 2010.

[10] B. Wikman, N. Solimannezhad, M. Oldenburg and H. Haggblad, "Wall friction coeficient estimation throught modelling of powder pressing experiment," *Powder Metallurgy,* pp. 132-138, 2000.

[11] P. Rendaz, "A study of stresses in powder compacted components during and after ejection," *International Journal of Solids and Structures,* pp. 759-775, 2001.

[12] A. Bejarano, M. Riera and J. Prado, "Simulation of the compaction process of a two-level powder metallurgical part," *Materials Processing Technology,* pp. 34-40, 2003.

[13] H. A. Al-Qureshi, M. R. F. Soares, D. Hotza, M. C. Alves and A. N. Klein, "Analyses of the fundamental Parameters of Cold Die Compaction of Powder Metallurgy," *Journal of Materials Processing Technology,* pp. 417-424, 2008.

[14] P. Moseley, “Numerical Implementation of a Drucker-Prager Plasticity Model,” Evanston,IL, 2010.

[15] A. Anandarajah, Computational Methods in Elasticity and Plasticity, Canada: Springer, 2010.

[16] K. N. Emmanuel, P. B. D. Reddy and E. Dr. Francois, “Theoretical Aspects of Classicl and Drucker-Prager Cap Models of Elasticity,” AIMS Internal Resources, Cape Town, South Africa, 2006.

[17] W. W., “A statistical distribution function of wide applicability,” *Journal of Applied Mechanics,* vol. 18, no. 3, pp. 293-297, 1951.

[18] A. Jayatilaka and K. Trusttrum, “Statistical approach to brittle fracture,” *Journal of Material Science,* vol. 12, no. 7, pp. 1426-1430, 1977.

[19] D. Harlow and T. Delph, “A Probability Model for Creep Fatigue Failure,” *Journal of Pressure Vessel Technology,* vol. 119, no. 1, pp. 45-51, 1997.

[20] Z. Lu, C. Liu, Z. Yue and Y. Xu, “Probabilistic safe analysis of the working life of a powder metallurgical turbine disc,” *Material Science & Engineering A,* vol. 395, no. 1-2, pp. 153-159, 2004.

[21] T. Senthilvelan, K. Raghukandan and A. Venkatraman, “Testing and Quality Standards for Powder Metallurgy Products,” *Materials and Manufacturing Processes,* pp. 37-41, 7 February 2007.

[22] D. Poquillon, V. Baco-Carles, P. Tailhades and E. Andrieu, “Cold compaction of iron powders--Relations between powder morphology and mechanical properties Part II. Bending tests: results and analysis,” *Powder Technology,* pp. 75-84, 2002.

[23] L. H. Han, P. R. Laity, R. E. Cameron and J. A. Elliott, “Density and plastic strain evaluations using small-andle X-ray scattering and finite element simulations for powder compacts of complex shape,” *Springer Science+Business Media, LLC,* no. 46, pp. 5977-5990, 2011.

[24] D. L. Logan, Finite Element Method, THOMSON, 2007.

[25] JWsuther, “Orthogonal Arrays,” jwsuther, 2005. [Online]. Available: http://www.me.mtu.edu/~jwsuther/doe2005/notes/orth_arrays.pdf. [Accessed 4 May 2012].

[26] O. C. a. H. Riedel, “Numerical simulation of metal powder die compaction with special consideration of cracking,” *Powder Metallurgy,* pp. 123-131, 2000.

[27] T. Sinha, J. S. Curtis, B. C. Hancock and C. Wassgren, “A study on the sensitivity of Drucker-Prager Cap model parameters during the decompression phase of powder compaction simulations,” *Powder Technology,* pp. 315-324, 2010.

[28] H. M. G. Hofstetter, “Computational plasticity of reinforced and prestressed concrete structures,”

Computational Mechanics, pp. 242-254, 1995.

[29] H. Y. X. Q. Jianzhong Wang, “Analysis of density and mechanical properties of high velocity compacted iron powder,” *Acta Metall,* vol. 22, pp. 447-453, 2009.

[30] H. Meftah, C. Hedi and G. Augustin, “Modeling the Powder Compaction Proecess Ising the Finite Element Method and Inverse Optimization,” *Powder Metallurgy,* pp. 631-647, 26 February 2011.